Atmos. Chem. Phys. Discuss., 15, 6277–6335, 2015
www.atmos-chem-phys-discuss.net/15/6277/2015/
doi:10.5194/acpd-15-6277-2015


Atmospheric Chemistry and Physics Discussions



# Evaluation of the MACC operational forecast system – potential and challenges of global near-real-time modelling with respect to reactive gases in the troposphere

**A. Wagner[1], A.-M. Blechschmidt[2], I. Bouarar[3,*], E.-G. Brunke[4], C. Clerbaux[3], M. Cupeiro[5], P. Cristofanelli[6], H. Eskes[7], J. Flemming[8], H. Flentje[1], M. George[3], S. Gilge[1], A. Hilboll[2], A. Inness[8], J. Kapsomenakis[9], A. Richter[2], L. Ries[10], W. Spangl[11], O. Stein[12], R. Weller[13], and C. Zerefos[9]**

[1]Deutscher Wetterdienst, Meteorologisches Observatorium Hohenpeissenberg, Hohenpeissenberg, Germany
[2]Institute of Environmental Physics, University of Bremen, Bremen, Germany
[3]Sorbonne Universités, UPMC Univ. Paris 06; Université Versailles St-Quentin; CNRS/INSU, LATMOS-IPSL, Paris, France
[4]South African Weather Service, Stellenbosch, South Africa
[5]National Meteorological Service, Ushuaia, Tierra del Fuego, Argentina



[6]National Research Council of Italy, ISAC, Bologna, Italy
[7]Royal Netherlands Meteorological Institute, De Bilt, the Netherlands
[8]European Centre for Medium-range Weather Forecasts, Reading, UK
[9]Academy of Athens, Research Centre for Atmospheric Physics and Climatology, Athens, Greece
[10]Federal Environment Agency, GAW Global Station Zugspitze/Hohenpeissenberg, Zugspitze 5, 82475 Zugspitze, Germany
[11]Umweltbundesamt GmbH, Air Pollution Control and Climate Change Mitigation, Vienna, Austria
[12]Forschungszentrum Jülich, IEK-8 (Troposphere), Jülich, Germany
[13]Alfred Wegener Institute, Bremerhaven, Germany
[*]now at: Max-Planck-Institut for Meteorology, Hamburg, Germany

Received: 7 October 2014 – Accepted: 25 January 2015 – Published: 4 March 2015

Correspondence to: A. Wagner (annette.wagner@dwd.de)

Published by Copernicus Publications on behalf of the European Geosciences Union.

**Abstract**

Monitoring Atmospheric Composition and Climate (MACC/MACCII) currently represents the European Union's Copernicus Atmosphere Monitoring Service (CAMS) (http://www.copernicus.eu/), which will become fully operational in the course of 2015. The global near-real-time MACC model production run for aerosol and reactive gases provides daily analyses and 5 day forecasts of atmospheric composition fields. It is the only assimilation system world-wide that is operational to produce global analyses and forecasts of reactive gases and aerosol fields. We have investigated the ability of the MACC analysis system to simulate tropospheric concentrations of reactive gases (CO, $O_3$, and $NO_2$) covering the period between 2009 and 2012. A validation was performed based on CO and $O_3$ surface observations from the Global Atmosphere Watch (GAW) network, $O_3$ surface observations from the European Monitoring and Evaluation Programme (EMEP) and furthermore, $NO_2$ tropospheric columns derived from the satellite sensors SCIAMACHY and GOME-2, and CO total columns derived from the satellite sensor MOPITT. The MACC system proved capable of reproducing reactive gas concentrations in consistent quality, however, with a seasonally dependent bias compared to surface and satellite observations: for northern hemispheric surface $O_3$ mixing ratios, positive biases appear during the warm seasons and negative biases during the cold parts of the years, with monthly Modified Normalised Mean Biases (MNMBs) ranging between −30 and 30 % at the surface. Model biases are likely to result from difficulties in the simulation of vertical mixing at night and deficiencies in the model's dry deposition parameterization. Observed tropospheric columns of $NO_2$ and CO could be reproduced correctly during the warm seasons, but are mostly underestimated by the model during the cold seasons, when anthropogenic emissions are at a highest, especially over the US, Europe and Asia. Monthly MNMBs of the satellite data evaluation range between −110 and 40 % for $NO_2$ and at most −20 % for CO, over the investigated regions. The underestimation is likely to result from a combination of errors concerning the dry deposition parameterization and certain limitations in the current emission inventories, together with an insufficiently established seasonality in the emissions.



## 1 Introduction

Reactive gases play an important role in tropospheric chemistry.

Carbon monoxide (CO) is part of a photo-chemically driven reaction sequence that links methane ($CH_4$), formaldehyde (HCHO), ozone ($O_3$), and the hydroxyl radical (OH). It also is a precursor of tropospheric ozone. Carbon monoxide has natural and anthropogenic sources (Seinfeld and Pandis, 2006). Its main sources are incomplete fossil fuel and biomass burning, but also the oxidation of anthropogenic and biogenic volatile organic compounds (VOCs).

High CO concentrations in the troposphere are found especially over the industrial regions of Europe, Asia and North America as well as over biomass burning regions in Africa. In the Northern Hemisphere the surface CO concentration peak appears around March with typical mixing ratios of around 150 parts per billion (ppb) measured at background stations (e.g., Stein et al., 2014). The Northern Hemisphere winter CO maximum results largely from a build-up of anthropogenic emissions, while in the Southern Hemisphere, biomass burning is the dominant contributor of CO in the boreal summer (July–October). In both hemispheres, reaction with OH leads to a minimum of CO in the summer months. In areas with large biogenic emissions (e.g., tropical rain forests), the oxidation of biogenic VOCs contributes strongly to the production of CO (Griffin et al., 2007).

Ozone in the troposphere is highly relevant for the Earth's climate, ecosystems, and human health (e.g., Cape, 2008; Mohnen et al., 2013; Selin et al., 2009). Due to its relatively short lifetime in the atmosphere when compared to carbon dioxide, ozone is often referred to as "short-lived climate forcer". It is the third largest contributor of anthropogenic greenhouse gas radiative forcing after carbon dioxide and methane (Forster et al., 2007) and it plays a crucial role in tropospheric chemistry as the main precur-

sor of the OH radical which determines the oxidation capacity of the troposphere (e.g., Seinfeld and Pandis, 2006; Cooper et al., 2014). As a toxic air pollutant, higher concentrations of $O_3$ can also affect human health (Bell et al., 2006). $O_3$ formation occurs in the troposphere mainly when nitric oxide (NO) and nitrogen dioxide ($NO_2$) (the sum of which is referred to as $NO_x$), CO, and VOCs react in the presence of sunlight. Thus, during spring and summer, high $O_3$ concentrations usually occur downwind of urban areas or over regions with intense biomass burning activity.

Nitric oxide (NO) and nitrogen dioxide ($NO_2$), exert a major influence on oxidation processes in the troposphere. NO rapidly reacts with $O_3$ to form $NO_2$. Nitrogen oxides have their sources in both anthropogenic processes (e.g., fossil fuel combustion) and natural processes (e.g., soil emissions and lightning). The lifetime of $NO_x$ comprises a few days in the free troposphere and less in the boundary layer. Concentrations are typically larger over land than over the oceans. The largest concentrations are found over industrial and urban regions of the Eastern US, California, Europe, China and Japan (e.g., Leue et al., 2001; Velders et al., 2001; Richter et al., 2005). Major sinks of $NO_x$ are reactions of $NO_2$ with OH to $HNO_3$, with $O_3$ to $NO_3$ at night and the formation of peroxyacyl nitrates as well as dry deposition (Inness et al., 2013; Penkett et al., 2011).

The EU-funded research project MACC/MACC-II – Monitoring Atmospheric Composition and Climate – is the basis of the Copernicus Atmosphere Monitoring Service. This service has been established by the EU to provide a range of products of societal and environmental value with the aim to help European governments respond to climate change and air quality problems. For the generation of atmospheric products, state-of-the-art atmospheric modelling is combined with assimilated satellite data (Hollingsworth et al., 2008, more general information about data assimilation can be found in e.g. Ballabrera-Poy et al., 2009 or Kalnay, 2003).

MACC-II provides reanalysis, monitoring products of atmospheric key constituents (e.g., Inness et al., 2013), as well as operational daily forecasting of greenhouse gases, aerosols and reactive gases (Benedetti et al., 2011; Stein et al., 2012) on



a global and on European-scale level, and derived products such as solar radiation. An important aim of the MACC system is to describe the occurrence, magnitude and transport pathways of disruptive events, e.g., volcanoes (Flemming and Inness, 2013), major fires (Huijnen et al., 2012; Kaiser et al., 2012) and dust storms (Cuevas et al., 2014). The product catalogue can be found on the MACC website, http://copernicus-atmosphere.eu. Within the MACC project there is a dedicated validation activity to provide up-to-date information on the quality of the reanalysis, daily analyses and forecasts. Validation reports are updated regularly and are available on the MACC websites.

The MACC global near-real-time (NRT) production model for reactive gases and aerosol has operated with data assimilation from September 2009 onwards, providing boundary conditions for the MACC regional air quality products (RAQ), and other downstream users. The model simulations also provide input for the stratospheric ozone analyses delivered in near-real-time by the MACC stratospheric ozone system (Lefever et al., 2014).

This paper investigates the potential and challenges of near-real-time modelling with the MACC analysis system between 2009 and 2012. We concentrate on this period because of the availability of validated independent observations (namely surface observations from the Global Atmosphere Watch Programme GAW, the European Monitoring and Evaluation Programme EMEP, as well as total column satellite data from the MOPITT, SCIAMACHY and GOME-2 sensors) that are used for comparison. In particular, we study the model's ability to reproduce the seasonality and absolute values of tropospheric CO and $NO_2$ as well as surface $O_3$ and CO. The impact of changes in model version, data assimilation and emission inventories on the model performance are examined and discussed.

The paper is structured in the following way: Sect. 2 contains a description of the model and the validation data sets as well as the applied validation metrics. Section 3 presents the validation results for CO, $NO_2$ and $O_3$. Section 4 encloses the discussion and Sect. 5 the conclusions of the paper.

## 2 Data and methods

### 2.1 The MACC model system in the 2009–2012 period

The MACC global products for reactive gases consist of a reanalysis performed for the years 2003–2012 (Inness et al., 2013) and the near-real-time analysis and forecast, largely based on the same assimilation and forecasting system, but targeting different user groups. The MOZART chemical transport model (CTM) is coupled to the Integrated Forecast System (IFS) of the European Centre for Medium–Range Weather forecast (ECMWF), which together represent the MOZART-IFS model system (Flemming et al., 2009 and Stein et al., 2012). An alternative analysis system has been set up based on the global CTM TM5 (Huijnen et al., 2010). Details of the MOZART version used in the MACC global products can be found in Kinnison et al., 2007 and Stein et al. (2011, 2012). In the simulation, the IFS and the MOZART model run in parallel and exchange several two- and three-dimensional fields every model hour using the OASIS4 coupling software (Valcke and Redler, 2006), thereby producing three-dimensional IFS fields for $O_3$, CO, $SO_2$, $NO_x$, HCHO, sea salt aerosol, desert dust, black carbon, organic matter, and total aerosol. The IFS provides meteorological data to MOZART. Data assimilation and transport of the MACC species takes place in IFS, while the whole chemical reaction system is calculated in MOZART.

The MACC_osuite is the global near-real-time MACC model production run for aerosol and reactive gases. Here, we have investigated only the MACC analysis. In contrast to the reanalysis, the MACC_osuite is a near-real-time run, which implies that it is only run once in near-real-time and may thus contain inconsistencies in e.g. the assimilated data. The MACC_osuite was based on the IFS cycle CY36R1 with IFS model resolution of approximately 100 km at 60 levels (T159L60) from September 2009 until July 2012. The gas-phase chemistry module in this cycle is based on MOZART-3 (Kinnison et al., 2007). The model has been upgraded, following updates of the ECMWF meteorological model and MACC-specific updates, i.e. in chemical data assimilation and with respect to the chemical model itself. Thus, from July 2012 on-



wards, the MACC_osuite has run with a change of the meteorological model to a new IFS cycle (version CY37R3), with an IFS model resolution of approximately 80 km at 60 levels (T255L60) and an upgrade of the MOZART version 3.5 (Kinnison et al., 2007; Emmons et al., 2011; Stein et al., 2013). This includes, amongst others, updated velocity fields for the dry deposition of $O_3$ over ice, as described in Stein et al. (2013).

A detailed documentation of system changes can be found at: http://www.copernicus-atmosphere.eu/oper_info/nrt_info_for_users/.

#### 2.1.1 Emission inventories and assimilated data sets

In the MACC_osuite, anthropogenic emissions go back to a merged RETRO-REAS inventory; biogenic emissions are taken from GEIA, both available in monthly resolution (Schultz et al., 2007). Fire emissions are based on a climatology derived from GFEDv2 (van der Werf et al., 2006) until April 2010, when fire emissions change to GFAS fire emissions (Kaiser et al., 2012). Between January 2011 and October 2011 there has been a fire emission reading error in the model, where, instead of adjusting emissions to the appropriate month, the same set of emissions have been read throughout this period.

After the model upgrade to the new cycle version CY37R3, in July 2012, the emission inventories changed from the merged RETRO-REAS and GEIA inventories, used in the previous cycle, to the MACCity anthropogenic and biogenic emissions (Granier et al., 2011) and (climatological) MEGAN-v2 (Guenther et al., 2006) emission inventories. Wintertime anthropogenic CO emissions are scaled up over Europe and North America (see Stein et al., 2014). Near-real-time fire emissions are taken from GFASv1.0 (Kaiser et al., 2012), for both gas-phase and aerosol.

In the MACC_osuite, the initial conditions for some of the chemical species are provided by data assimilation of atmospheric composition observations from satellites (see Benedetti et al., 2009; Inness et al., 2009, 2013; Massart et al., 2014). Table 2 lists up the assimilated data products. From September 2009 to June 2012, $O_3$ total columns of the MLS and SBUV-2 instruments are assimilated, as well as OMI and SCIAMACHY

total columns (the latter only until March 2012, when the European Space Agency lost contact with the ENVIronmental SATellite ENVISAT). CO total columns are assimilated from the IASI sensor and aerosol total optical depth is assimilated from the MODIS instrument. After the model cycle update in July 2012, data assimilation also contains OMI tropospheric columns of $NO_2$ and $SO_2$, as well as CO MOPITT total columns. The CO total columns retrieved by MOPITT and IASI instruments have a relatively similar seasonality, but there is a systematic difference with MOPITT CO being higher over most regions in the Northern Hemisphere, especially during winter and spring. George et al. (2015) investigated the differences between MOPITT and IASI, and showed the impact of a priori information on the retrieved measurements.

Tables 1 and 2 summarize the setup and data assimilation of the MACC_osuite.

### 2.2 Validation data and methodology

In this study, mainly the same evaluation data sets have been used as during the MACC near-real-time validation exercise. This implies some discontinuities in the evaluations, e.g. the substitution of SCIAMACHY data with GOME-2 data after the loss of the ENVISAT sensor or an exclusion of MOPITT satellite data after the start of its assimilation into the model. The continuous process of updating and complementation of data sets in databases requires the selection and definition of an evaluation data set at some point. The comparatively small inconsistencies between our data sets are considered to have a negligible impact on the overall evaluation results.

#### 2.2.1 GAW surface $O_3$ and CO observations

The Global Atmosphere Watch (GAW) programme of the World Meteorological Organization (WMO) has been established to provide reliable long-term observations of the chemical composition and physical properties of the atmosphere, which are relevant for understanding atmospheric chemistry and climate change (WMO, 2013). GAW tropospheric $O_3$ measurements are performed in a way to be suitable for the detection



of long-term regional and global changes. Furthermore, the GAW measurement programme focuses on observations, which are regionally representative and should be free from influence of significant local pollution sources and suited for the validation of global chemistry climate models (WMO 2007a). Detailed information on GAW and GAW related $O_3$ and CO measurements can be found in WMO (2007b, 2010, 2013).

Tropospheric hourly $O_3$ and CO data have been downloaded from the WMO/GAW World Data Centre for Greenhouse Gases (WDCGG) for the period between September 2009 and December 2012 (status of download: July 2013). Our evaluation includes 29 stations with surface observations for CO and 50 stations with surface observations for $O_3$. Table 3 lists the geographic coordinates and altitudes of the individual stations. Being a long-term data network, the data in the database is provided with a temporal delay of approximately 2 years. As the data in the database becomes sparse towards the end of the validation period, near-real-time observations, as used in the MACC-project for near-real-time validation, presented on the MACC website, have been included to complement the validation data sets. For the detection of long-term trends and year-to-year variability, the data quality objectives (DQOs) for CO in GAW measurements are set to a maximum uncertainty of ±2 ppb and to ±5 ppb for marine boundary layer sites and continental sites that are influenced by regional pollution and to ±1 ppb for ozone (WMO, 2012, 2013).

For the evaluation with GAW station data, 6 hourly values (00:00, 06:00, 12:00, 18:00 UTC) of the analysis mode have been extracted from the model and are matched with hourly observational GAW station data. Model mixing ratios at the stations' location have been linearly interpolated from the model data in the horizontal. In the vertical, modelled gas mixing ratios have been extracted at the model level, which is closest to the GAW stations' altitude. Validation scores (see Sect. 2.3) have been calculated for each station between the 6 hourly model analysis data and the corresponding observational data for the entire period (September 2009–December 2012) and as monthly averages.

### 2.2.2 EMEP surface $O_3$ observations

The European Monitoring and Evaluation Programme (EMEP) is a scientifically based and policy driven programme under the Convention on Long-Range Transboundary Air Pollution (CLRTAP) for international co-operation to solve transboundary air pollution problems. Measurements of air quality in Europe have been carried out under the EMEP since 1977.

A detailed description of the EMEP measurement programme can be found in Tørseth et al. (2012). The surface hourly ozone data between September 2009 and December 2012 have been downloaded from the EMEP data web-page (http://www.nilu.no/projects/ccc/emepdata.html). For the validation, only stations meeting the 75 % availability threshold per day and per month are taken into account. The precision is close to 1.5 ppb for a 10 s measurement. More information about the ozone data quality, calibration and maintenance procedures can be found in Aas et al. (2000).

For comparison with EMEP data, 3 hourly model values (00:00, 03:00, 06:00, 12:00, 15:00, 18:00, 21:00 UTC) of the analysis mode have been chosen, in order to be able to evaluate day and night time performance of the model separately. Gas mixing ratios have been extracted from the model and are matched with hourly observational surface ozone data at 124 EMEP stations in the same way as for the GAW station data. The EMEP surface ozone values and the interpolated surface modeled values are compared on a monthly basis for the latitude bands of 30–40° N (Southern Europe), 40–50° N (Central Europe) and 50–70° N (Northern Europe). For the identification of differences in the MACC_osuite performance between day and night time, the MACC_osuite simulations and the EMEP observations for the three latitude bands have been additionally separated into day-time (12:00–15:00 Local Time LT) and night-time (00:00–03:00 LT) intervals.



### 2.2.3 MOPITT CO total column retrievals

The MOPITT (Measurement Of Pollution In The Troposphere) instrument is mounted on board the NASA EOS Terra satellite and provides CO distributions at the global scale (Deeter et al., 2004). MOPITT has a horizontal resolution of 22 km × 22 km and allows global coverage within 3 days. The data used in this study corresponds to CO total columns from version 5 (V5) of the MOPITT thermal infrared (TIR) product level 3. This product is available via the following web server: http://www2.acd.ucar.edu/mopitt/products. Validation of the MOPITT V5 product against in-situ CO observations showed a mean bias of $0.06 \times 10^{18}$ molecules cm$^{-2}$ (Deeter et al., 2013). Following the recommendation in the users' guide, (www.acd.ucar.edu/mopitt/v5_users_guide_beta.pdf), the MOPITT data were averaged by taking into account their relative errors provided by the Observation Quality Index (OQI).

Also, in order for better data quality we used only daytime CO data since retrieval sensitivity is greater for daytime rather than nighttime overpasses. A further description of the V5 data is presented in Deeter et al. (2013) and Worden et al. (2014).

For the validation, the model CO profiles ($X$) were transformed by applying the MOPITT averaging kernels ($A$) and the a priori CO profile ($X_a$) according to the following equation (Rodgers, 2000) to derive the smoothed profiles $X^*$ appropriate for comparison with MOPITT data:

$$X^* = X_a + A(X - X_a)$$

Details on the method of calculation are referred to in Deeter et al. (2004) and Rodgers (2000). The averaging kernels indicate the sensitivity of the MOPITT measurement and retrieval system to the true CO profile, with the remainder of the information set by the a priori profile and retrieval constraints (Emmons, 2009; Deeter et al., 2010). The model CO total columns used in the comparison with MOPITT observations, have been calculated using the averaging kernel smoothed profiles $X^*$ which have the same vertical resolution and a priori dependence as the MOPITT retrievals. For the evaluation,

8 regions are defined (see Fig. 1): Europe, Fires-Alaska, Fires-Siberia, North Africa, South Africa, South Asia, East Asia and the United States.

The model update in July 2012 includes an integration of MOPITT CO total columns in the model's data assimilation system. With this, the MOPITT validation data has lost its independency for the rest of the validation period and MOPITT validation data has thus only been used until June 2012 for validation purposes.

#### 2.2.4 SCIAMACHY and GOME-2 $NO_2$ satellite observations

The SCanning Imaging Absorption spectroMeter for Atmospheric CHartographY (SCIAMACHY; Bovensmann et al., 1999) onboard the ENVISAT and the Global Ozone Monitoring Experiment-2 (GOME-2; Callies et al., 2000) onboard the Meteorological Operational Satellite-A (MetOp-A) comprise UV-vis and near-infrared sensors designed to provide global observations of atmospheric trace gases.

In this study, the tropospheric $NO_2$ column data set described in Hilboll et al. (2013a) has been used. In short, the measured radiances are analysed using Differential Optical Absorption Spectroscopy (DOAS), (Platt and Stutz, 2008) in the 425–450 nm wavelength window (Richter and Burrows, 2002). The influence of stratospheric $NO_2$ air masses has been accounted for using the algorithm detailed by Hilboll et al. (2013b), using stratospheric $NO_2$ fields from the B3dCTM model (Sinnhuber at al., 2003a; Sinnhuber et al., 2003b; Winkler et al., 2008). Tropospheric air mass factors have been calculated with the radiative transfer model SCIATRAN (Rozanov et al., 2005). Only measurements with FRESCO+ algorithm (Wang et al., 2008) cloud fractions of less than 20 % are used.

Tropospheric $NO_2$ vertical column densitiy (VCD) from the MACC_osuite is compared to tropospheric $NO_2$ VCD from GOME-2 and SCIAMACHY. As the European Space Agency lost contact with ENVISAT in April 2012, GOME-2 data is used for model validation from 1 April 2012 onwards, while SCIAMACHY data is used for the remaining time period (September 2009 to March 2012). Satellite observations are gridded to the



horizontal model resolution, i.e. 1.875° for IFS cycle CY36R1 (September 2009–June 2012) and 1.125° for cycle CY37R3 (July 2012–December 2012).

A few processing steps are applied to the MACC_osuite data to account for differences to the satellite data such as observation time. Firstly, model data are vertically integrated to tropospheric $NO_2$ VCDs by applying National Centers for Environmental Prediction (NCEP) reanalysis (Kalnay et al., 1996) climatological tropopause pressure shown in Fig. 1 of Santer et al. (2003). Secondly, simulations are interpolated linearly to the SCIAMACHY equator crossing time (roughly 10:00 LT). This most likely leads to some minor overestimation of model $NO_2$ VCDs compared to GOME-2 data, as the equator crossing time for GOME-2 is about 09:30 LT. Moreover, only model data for which corresponding satellite observations exist are considered. For the evaluation, the same regions have been used as for MOPITT (Fig. 1), except for Siberia and Alaska. In contrast to MOPITT data, no averaging kernel is applied.

### 2.3 Validation metrics

A comprehensive model evaluation requires the selection of validation metrics that provide complementary aspects of model performance. The following metrics have been used in the evaluation:

**Modified Normalized Mean Bias MNMB**

$$\mathrm{MNMB} = \frac{2}{N}\sum_i \frac{f_i - o_i}{f_i + o_i} \quad (1)$$

**Root Mean Square Error RMSE**

$$\mathrm{RMSE} = \sqrt{\frac{1}{N}\sum_i (f_i - o_i)^2} \quad (2)$$

**Correlation Coefficient**

$$R = \frac{\frac{1}{N}\sum_i \left(f_i - \overline{f}\right)\left(o_i - \overline{o}\right)}{\sigma_f \sigma_o} \quad (3)$$

where: $N$ is the number of observations, $f$ are the modelled analysis and $o$ the observed values, $\overline{f}$ and $\overline{o}$ are the mean values of the analysis and observed values and $\sigma_f$ and $\sigma_o$ are the corresponding SDs.

The validation metrics above have been chosen to provide complementary aspects of model performance. The modified normalized mean bias (e.g. Elguindi et al., 2010) ranges between −2 and 2 and is very useful to check whether there is a negative or positive deviation between model and observations. When multiplied by 100 %, it can be interpreted as a percentage bias. The advantage of the MNMB is that it varies symmetrically with respect to under- and overestimation and is robust with respect to outliers. However, when calculated over longer time periods, a balance in model error, with model over-and underestimation compensating each other, can lead to a small MNMB for the overall period. For this reason, it is important to additionally consider an absolute measure, such as the RMSE. However, it has to be noted that the RMSE is strongly influenced by larger values and outliers, due to squaring. The correlation coefficient $R$ can vary between 1 (perfect correlation) and −1 (negative correlation) and is an important measure to check the linearity between model and observations.

## 3 Results

### 3.1 Evaluation of $O_3$ mixing ratios

The evaluation of the MACC_osuite run with $O_3$ from GAW surface observations (described in Sect. 2.2.1) demonstrates good agreement in absolute values and seasonality for most regions. Figure 11 shows a map with MNMB evaluations for 50 GAW



stations. Large negative MNMBs over the whole period September 2009 to December 2012 (−30 to −82 %) are observed for stations located in Antarctica (Neumayer – NEU, South Pole – SPO, Syowa – SYO and Concordia – CON) whereby $O_3$ surface mixing ratios are strongly underestimated by the model. For stations in the far north (Barrow – BAR, Alaska and Summit – SUM, Denmark), the MACC_osuite exhibits similar underestimated values of up to −35 % for the whole evaluation period. The time series plots for Arctic and Antarctic stations (e.g. Summit – SUM, Neumayer – NEU and South Pole – SPO) in Fig. 13 show that an underestimation visible in these regions has been remedied and model performance improved with an updated dry deposition parameterization over ice, which has been introduced with the new model cycle in July 2012 (see Sect. 2.1).

Large positive MNMBs (up to 50 to 70 %, Fig. 11) are observed for stations that are located in or nearby cities and thus exposed to regional sources of contamination (Iskrba – ISK Slovenia, Tsukuba – TSU, Japan, Cairo – CAI, Egypt). In tropical and subtropical regions, $O_3$ surface mixing ratios are systematically overestimated (by about 20 % on average) during the evaluation period. The time series plots for tropical and subtropical stations (e.g. for Ragged Point – RAG, Barbados and Cape Verde Observatory, Cape Verde – CVO, Fig. 13) reveal a slight systematic positive offset throughout the year, however with high correlation coefficients (0.6 on average).

For GAW stations in Europe, the evaluation of the MACC_osuite for the whole period shows MNMBs between −80 and 67 %. Large biases appear only for 2 GAW stations located in Europe: Rigi – RIG, Switzerland (−80 %), located near mountainous terrain and Iskrba – ISK, Slovenia (67 %). For the rest of the stations MNMBs lie between 22 and −30 %. RMSEs range between 7 and 35 ppb (15 ppb on average). Again results for Iskrba – ISK and Rigi – RIG show the largest errors. All other stations show RMSEs between 7 and 20 ppb. Correlation coefficients here range between 0.1 and 0.7 (with 0.5 on average). Table 6 summarizes the results for all stations individually.

Monthly MNMBs (see Fig. 12) show a seasonally varying bias, with positive MNMBs occurring during the northern summer months (with global average ranging between 5

and 29 % during the months June and October), and negative MNMBs during the northern winter months (between −2 and −33 % during the months December to March). These deviations partly cancel each other out in MNMB for the whole evaluation period. For the RMSEs, maximum values also occur during the northern summer months with global average ranging between 11 and 16 ppb for June to September. The smallest errors appear during the northern winter months (global average falling between 8 and 10 ppb for December and January). The correlation does not show a distinct seasonal behaviour (see Fig. 12).

The time series plots in Fig. 13 show that the seasonal cycle of $O_3$ mixing ratios with maximum concentrations during the summer months and minimum values occurring during winter times for European stations (e.g. Monte Cimone – MCI, Italy, Kosetice – KOS, Czech Republic, and Kovk – KOV, Slovenia), could well be reproduced by the model, although there is some overestimation in summer resulting mostly from observed minimum concentrations that are not captured correctly by MACC_osuite, (Kosetice – KOS, Czech Republic, and Kovk – KOV, Slovenia).

The validation with EMEP surface ozone observations (described in Sect. 2.2.2) in three different regions in Europe for the period September 2009 to December 2012 likewise confirms the behaviour of the model to overestimate $O_3$ mixing ratios during the warm period and underestimate $O_3$ concentrations during the cold period of the year (see Fig. 14). The positive bias (May–November) is between −9 and 56 % for northern Europe and Central Europe and between 8 and 48 % for Southern Europe. Negative MNMBs appear, in accordance with GAW validation results, during the winter-spring period (December–April) ranging between −48 and −7 % for EMEP stations in northern Europe (exception: December 2010 with 25 %), between −1 and −39 % in central Europe (exception: December 2012 with 31 %), whereas in southern Europe, deviations are smaller and remain mostly positive (between −8 and 9 %) in winter (exception: December 2012 with 37 %). The evaluation of the diurnal $O_3$ cycle (Fig. 15) shows that for northern Europe larger biases appear during night time. For central Europe and





southern Europe night-time biases are larger during cold periods (December–April), whereas during warm periods (May–November) larger biases appear during day time.

### 3.2 Evaluation of carbon monoxide

The evaluation of the MACC_osuite with surface observations of 29 GAW stations (described in Sect. 2.2.1) shows that over the whole period September 2009 to December 2012, CO mixing ratios could be reproduced with an average Modified Normalized Mean Bias (MNMB, see Sect. 2.3) of −10 %. The MNMBs for all stations range between −50 and +30 %. MNMBs exceeding ±30 % appear for stations that are either located in or nearby cities and thus exposed to regional sources of contamination (Kosetice – KOS, Czech Republic) or are located in or near complex mountainous terrain (Rigi – RIG, Switzerland, BEO Moussala – BEO, Bulgaria) which is not resolved by the topography of the global model. Root Mean Square Errors (RMSEs, see Sect. 2.3) fall between 12 and 143 ppb (on average 48 ppb) for all stations during the validation period, but for only four stations (Rigi – RIG, Kosetice – KOS, Payerne – PAY, Switzerland and BEO Moussala – BEO, all located in Europe) do the RMSEs exceed 70 ppb. Correlation coefficients from the comparison with GAW station data calculated over the whole time period range between 0 and 0.8 (on average 0.4), with only four stations showing values smaller than 0.2 (Rigi – RIG, Moussala – BEO, East Trout Lake – ETL and Lac la Biche – LAC (the latter two located in Canada). All results are listed in Table 4.

Considering the monthly MNMBs, RMSEs and correlation coefficients, it can be seen that during the northern summer months, June to September, MNMBs are small (absolute differences less than 5 %), see Fig. 2. Negative MNMBs (up to −35 %) and larger RMSEs (up to 72 ppb) appear during the northern winter months, November to March, when anthropogenic emissions are at a highest, especially for the US, northern latitudes and Europe. Correlation coefficients are between 0.1 and 0.5 and do not show a distinct seasonal behaviour (see Fig. 2). The rather low correlation coefficient is re-

lated to mismatches in the strong short-term variability seen in both the model and the measurements.

The time series plots in Fig. 3 demonstrate that the annual CO cycle could to a large degree be reproduced correctly by the model with maximum values occurring during the winter period and minimum values appearing during the summer season. However, the model shows a negative offset during the winter period. Seasonal air mass transport patterns that lead to regular annual re-occurring CO variations could be reproduced for GAW stations in East Asia: the time series plots for Yonagunijima – YON and Minamitorishima – MNM station, Japan (Fig. 3) show that the drop of CO, associated with the air mass change from continental to cleaner marine air masses after the onset of the monsoon season during the early summer months, is captured by the MACC_osuite. Deterioration in all scores is visible during December 2010 in the time series plots of several stations (e.g. Jungfraujoch – JFJ, and Sonnblick – SBL, Fig. 3). This is likely a result of changes in the processing of the L2 IASI data and a temporary blacklisting of IASI data (to avoid model failure) in the assimilation.

The comparison with MOPITT satellite CO total columns between October 2009 and June 2012 (described in Sect. 2.2.3) shows a good qualitative agreement of spatial patterns and seasonality. The MNMBs for 8 regions are listed in Fig. 4 and range between 14 and −22 %. The seasonality of the satellite observations is captured well by the MACC_osuite over Asia and Africa, with MNMBs between −6 and 9 % (North Africa), −12 and 8 % (South Africa), −11 and 12 % (East Asia), and −3 and 14 % (South Asia). The largest negative MNMBs appear during the winter periods, especially from December 2010 to May 2011 and from September 2011 to April 2012, for Alaska and Siberia and for the US and Europe (MNMBs up to −22 %), which coincides with large differences between MOPITT and IASI satellite data (see Fig. 5). On the global scale the average difference between the IASI and MOPITT total columns is less than 10 % (George et al., 2009), and there is a close agreement of MOPITT and IASI for S. Asia and Africa (see Fig. 4). However, larger differences between MOPITT and IASI data appear during the northern winter months over Alaska, Siberia, Europe and the US.



These differences can be mainly explained by the use of different a priori assumptions in the IASI and MOPITT retrieval algorithms (George et al., 2015). Indeed, the Fast Optimal Retrievals on Layers for IASI (FORLI) software (IASI) is using a single a priori CO profile (with an associated variance-covariance matrix) whereas the MOPITT retrieval algorithm is using a variable a priori, depending on time and location. George et al. (2015) show that differences above Europe and the US in January and December (for a 5 year study) decrease by a factor of 2 when comparing IASI with a modified MOPITT product using the IASI single a priori. Between January 2011 and October 2011 there has also been a reading error in the fire emissions that contributes to larger MNMBs during this period (see Sect. 2.1.1).

### 3.3 Evaluation of tropospheric nitrogen dioxide

Figure 6 shows daily tropospheric $NO_2$ VCD averaged over six regions from September 2009 to December 2012. Overall, spatial distribution and magnitude of tropospheric $NO_2$ observed by GOME-2 and SCIAMACHY are well reproduced by the model. This indicates that emission patterns and $NO_x$ photochemistry are reasonably well represented by the model. However, the model underestimates tropospheric $NO_2$ VCDs over industrial areas in Europe, East China, Russia, and South East Africa compared to satellite data. This could imply that anthropogenic emissions from RETRO-REAS are underestimated in these regions, or that the lifetime in the model is too short. The model simulates larger $NO_2$ VCD maxima over Central Africa, which mainly originate from wild fires. It remains unclear if GFEDv2/GFAS fire emissions are too high here or if $NO_2$ fire plumes closer to the ground cannot be seen by the satellites due to light scattering by biomass burning aerosols (Leitao et al., 2010). In the Northern Hemisphere, background values of $NO_2$ VCD over the ocean are lower in the simulations than in the satellite data. The same is true for the South Atlantic Ocean to the west of Africa (see Fig. 7). This might suggest complex processes involving $NO_2$ transport or chemistry, or to inaccuracies in the bias correction applied in the satellite retrieval.

Monthly means of tropospheric $NO_2$ VCD averaged over different regions are presented in Fig. 8. A time series of the MNMB and RMSE is shown in Figs. 9 and 10. Table 5 summarizes the statistical values derived over the whole time period. High anthropogenic emissions occur over the United States, Europe, South Asia and East Asia compared to other regions on the globe (e.g., Richter et al., 2005). In principle, the MACC_osuite catches the pattern of satellite $NO_2$ VCD over these regions. However, the model tends to underestimate $NO_2$ VCDs throughout the whole time period investigated here. The negative bias is most pronounced over East Asia with a modelled mean $NO_2$ VCD for September 2009 to December 2012 of about $3.74 \times 10^{15}$ molec cm$^{-2}$ lower than that derived from satellite measurements (see Table 5).

Considering monthly values, the MACC_osuite strongly underestimates magnitude and seasonal variation of satellite $NO_2$ VCD over East Asia (MNMBs between −40 and −110 % and RMSE between $1 \times 10^{15}$ molec cm$^{-2}$ and $14 \times 10^{15}$ molec cm$^{-2}$ throughout the whole time period). A change in the modelled $NO_2$ values is apparent in July 2012 when the emission inventories changed and the agreement with the satellite data improved for South and East Asia but deteriorated for the US and Europe. This results in a drop of MNMBs (Fig. 9) for Europe and the US with values approaching around −60 % by the end of 2012. Nevertheless, correlations between daily satellite and model data derived for the whole time period (see Table 5) are high for East Asia (0.840), South Asia (0.744), Europe (0.781), and lower, but still rather high, for the US (0.567).

The North African and South African regions are strongly affected by biomass burning (Schreier et al., 2013). Magnitude and seasonality of daily and monthly tropospheric $NO_2$ VCDs (Figs. 6 to 8) are rather well represented by the model, apart from January 2011 to October 2011, due to difficulties in reading fire emissions for this time period (see Sect. 2.1.1). The latter results in large absolute values of the MNMB (Fig. 9) and large RMSEs (Fig. 10) between January 2011 and October 2011 compared to the rest of the time period. As for other regions investigated in this section, mean values of simulated daily tropospheric $NO_2$ VCDs over North Africa and South Africa between



September 2009 and December 2012 are lower than the corresponding satellite mean values (see Table 5). The correlation between daily model and satellite data over the whole time period is 0.606 for South Africa but only 0.455 for North Africa, respectively. It should be investigated in future studies, if this difference in model performance for the African regions is due to meteorology, chemistry or emissions.

## 4 Discussion

The MACC_osuite model realistically reproduces CO and $NO_2$ total columns over most of the evaluated regions with monthly MNMBs falling between 10 and −20 % (CO) and between 40 and −110 % for $NO_2$. There is a close agreement of modelled CO total columns and satellite observations for Africa and South Asia throughout the evaluation period. $NO_2$ total columns agree well with satellite observations over the United States, South Asia and North Africa. However, there is a negative offset compared to the observational CO data over Europe and North America and for $NO_2$ over Europe and East Asia. The largest deviations occur during the winter season when the observed CO and $NO_2$ concentrations are at a highest. The evaluation with GAW CO data accordingly shows a wintertime negative bias of up to −35 % at the surface for stations in Europe and the US. A general underestimation of CO from global models in the Northern Hemisphere has been described by various authors (e.g., Shindell et al., 2006; Naik et al., 2013). According to Stein et al. (2014) this underestimation likely results from a combination of errors in the dry deposition parameterization and certain limitations in the current emission inventories. The latter include too low anthropogenic CO emissions from traffic or other combustion processes and missing anthropogenic VOC emissions in the emission inventories together with an insufficiently established seasonality in the emissions. An additional reason for the apparent underestimation of emissions in MACCity may be an exaggerated downward trend in the RCP8.5 (Representative Concentration Pathways) scenario in North America and Europe between 2000 and 2010, as this scenario was used to extrapolate the MACCity emissions from

their bench mark year, i.e. 2000. The quality of the emission inventory is even more crucial for short lived reactive species such as $NO_2$, where model results depend to a large extent on emission inventories incorporated in the simulations. This is highlighted by the deterioration of agreement between model results and satellite data for the US in July 2012 when anthropogenic emissions were changed from RETRO-REAS to MACCity. This change led to an increasing negative bias in $NO_2$ over Europe and North America and to an improvement for South and East Asia (see Fig. 9). A deterioration in MNMBs associated with the fire emissions is visible between January 2011 and October 2011 over regions with heavy fire activity (South Africa and East Asia), and goes back to a temporary error in the model regarding the reading of fire emissions (see Figs. 6 and 8).

Particular challenges for an operational forecast system are regions with rapid changes in emissions such as China, where inventories need to be extrapolated to obtain reasonable trends. A large underestimation of $NO_2$ in China especially in winter has been reported for other CTMs in previous publications (He et al., 2007; Itahashi et al., 2014). The latter has been linked to an underestimation of $NO_x$ and VOC emissions, unresolved seasonality in the emissions and expected non-linearity of $NO_x$ chemistry. For CO, uncertainties in the evaluation also include the retrieved amount of CO total columns between IASI and MOPITT. These vary with region, with IASI showing lower CO concentrations in several regions (Alaska, Siberia, Europe and the US) during the northern winter months, which possibly contribute to the deviations observed between the modelled data and MOPITT satellite data. These differences can primarily be explained by the use of different a priori assumptions in the IASI and MOPITT retrieval algorithms (George et al., 2015). On a global scale however, the average difference between the IASI and MOPITT total columns is less than 10 % (George et al., 2009).

The validation of global $O_3$ mixing ratios with GAW observations at the surface levels showed that the MACC_osuite could generally reproduce the observed annual cycle of ozone mixing ratios. Model validation with surface data shows global average



monthly MNMBs between −30 and 30 % (GAW) and for Europe between −50 and 60 % (EMEP). The bias between measured $O_3$ surface mixing ratios and the MACC_osuite is seasonally dependent, with an underestimation of the observed $O_3$ mixing ratios during the northern winter season and an overestimation during the summer months.

The validation of the diurnal cycle for Northern and Central Europe shows larger negative MNMBs in the winter months during night time than day time (Fig. 15), so that the negative bias in winter could be attributed to the simulation of vertical mixing at night, also described by Ordoñez (2010) and Schaap (2008), which remains a challenge in the model. The systematic underestimation of $O_3$ mixing ratios throughout the year for high latitude northern regions and Antarctica has its origin in an overestimation of the $O_3$ dry deposition velocities over ice. With the implementation of the new model cycle and MOZART model version, which includes updated velocity fields for the dry deposition of $O_3$, as described in Stein et al. (2013), the negative offset in the MACC_osuite model has been remedied for high latitude regions from July 2012 onwards (see the time series plots for the South Pole station – SPO and Neumayer – NEU in Fig. 13). The overestimation of $O_3$ mixing ratios for the northern hemispheric summer months is a well-known issue and has been described by various model validation studies (e.g., Brunner et al., 2003; Schaap et al., 2008; Ordoñez et al., 2010; Val Martin et al., 2014). Inadequate ozone precursor concentrations and aerosol induced radiative effects (photolysis) have been frequently identified as being the main factors. The time series plots in Fig. 13, however, demonstrate that the minimum concentrations in particular are not captured by the model during summer. Possible explanations include a general underestimation of NO titration which especially applies to stations with urban surroundings and strong sub-grid scale emissions (e.g. Tsukuba – TSU Fig. 13), including difficulties by the global model to resolve NO titration in urban plumes.

It also seems likely that dry deposition at wet surfaces in combination with the large surface sink gradient due to nocturnal stability cannot be resolved with the model's vertical resolution. In regions such as Central and Southern Europe (Fig. 15) where day time biases exceed night time biases, the overestimation of $O_3$ might be related

to an underestimation of day-time dry deposition velocities: Val Martin et al. (2014) describe a reduction of the summertime $O_3$ model bias for surface ozone after the implementation of adjustments in stomatal resistances in the MOZART model's dry deposition parameterization.

## 5 Conclusions

The MACC_osuite is the near-real-time MACC model analysis run for aerosol and global reactive gases. This model run proved capable of reproducing CO and $NO_2$ total columns over most of the evaluated regions, however with a negative offset compared to the observational data for CO over Europe and North America and for $NO_2$ over Europe and East Asia. It has shown for CO and $NO_2$, that the emission inventories play a crucial role for the quality of model results and remain a challenge for near-real-time modelling, especially for regions with rapid changes in emissions.

The validation of global $O_3$ mixing ratios with GAW observations at the surface showed that MACC_osuite could mostly reproduce the observed annual cycle of ozone mixing ratios, however with a seasonally dependent bias, resulting from difficulties in the simulation of vertical mixing at night and deficiencies in the model's dry deposition parametrization. Temporary inconsistencies in the assimilated satellite data and fire emissions showed only a minor impact on the overall quality of model results.

The MACC NRT system is constantly evolving. A promising step in its model development is the on-line integration of modules for atmospheric chemistry in the IFS, currently being tested for implementation in the MACC_osuite. In contrast to the coupled model configuration as used in this paper, the on-line integration in the Composition IFS (C-IFS) provides major advantages; apart from an enhanced computational efficiency, C-IFS promises an optimization of the implementation of feedback processes between gas-phase/aerosol chemical processes and atmospheric composition and meteorology, which is expected to improve the modelling results for reactive gases. Additionally, C-IFS will be available in combination with different CTMs, (MOZART and TM5), which



will help to explain whether deviations between model and observations go back to deficiencies in the chemistry scheme of a model.

*Acknowledgements.* This work has been carried out in the framework of the MACC and MACC-II projects, funded under the EU Seventh Research Framework Programme for research and technological development. The authors thank the MACC validation and reactive gas subproject teams for the fruitful discussions. Model simulations were carried out using the ECMWF supercomputer. We wish to acknowledge the provision of GAW hourly station data from the World Data Centre of Greenhouse Gases (WDCGG) and hourly EMEP station data from the NILU database. Specifically, we like to thank: the CSIRO Oceans and Atmosphere Flagship for making the data freely available and the Australian Bureau of Meteorology for continued operation and support of the Cape Grim station. We also like to thank Izaña Atmospheric Research Center (AEMET) for providing CO and $O_3$ data. Special thanks to the providers of NRT data to the MACC project, namely: Institute of Atmospheric Sciences and Climate (ISAC) of the Italian National Research Council (CNR), South African Weather Service, The University of York and National Centre for Atmospheric Science (NCAS (AMF)) (UK), and the Instituto Nacional de Meteorologia e Geofisica (INMG) (Cape Verde), National Air Pollution Monitoring Network (NABEL) (Federal Office for the Environment FOEN and Swiss Federal Laboratories for Materials Testing and Research EMPA), Japan Meteorological Agency (JMA), Alfred Wegener Institute, Umweltbundesamt (Austria), National Meteorological Service (Argentina), Umweltbundesamt (UBA, Germany). We thank the National Center for Atmospheric Research (NCAR) MOPITT science team and the NASA Langley Research Center, Atmospheric Science Data Center (ASDC), for producing and archiving the MOPITT CO product. IASI has been developed and built under the responsibility of the Centre National D'Etudes Spatiales (CNES, France). We are grateful to Juliette Hadji-Lazaro and the UBL/LATMOS IASI team for establishing the IASI-MACC near real time processing chain. We wish to acknowledge that SCIAMACHY lv1 (level 1) radiances were provided to the Institute of Environmental Physics, University of Bremen by ESA through DLR/DFD.

## References

Aas, W., Hjellbrekke, A.-G., and Schaug, J.: Data quality 1998, quality assurance and field comparisons, Kjeller, Norwegian Institute for Air Research (EMEP/CCC-Report 6/2000), 2000.

Ballabrera-Poy, J., Kalnay, E., and Yang, S.: Data assimilation in a system with two scales – combining two initialization techniques, Tellus A, 61, 539–549, doi:10.1111/j.1600-0870.2009.00400.x, 2009.

Bell, M. L., Peng, R. D., and Dominici, F.: The exposure–response curve for $O_3$ and risk of mortality and the adequacy of current $O_3$ regulations, Environ. Health Persp., 114, 532–536, 2006.

Benedetti, A., Morcrette, J.-J., Boucher, O., Dethof, A., Engelen, R. J., Fisher, M., Flentje, H., Huneeus, N., Jones, L., Kaiser, J. W., Kinne, S., Mangold, A., Razinger, M., Simmons, A. J., Suttie, M., and the GEMS-AER team: Aerosol analysis and forecast in the European Centre for Medium-Range Weather Forecasts Integrated Forecast System: data assimilation, J. Geophys. Res., D13205, 114, doi:10.1029/2008JD011115, 2008.

Benedetti, A., Kaiser, J. W., and Morcrette, J.-J:. [Global Climate] Aerosols [in "State of the Climate in 2010"], B. Am. Meteorol. Sci., 92, S65–S67, 2011.

Bovensmann, H., Burrows, J. P., Buchwitz, M., Frerick, J., Noël, S., Rozanov, V. V., Chance, K. V., and Goede, A. P. H.: SCIAMACHY: mission objectives and measurement modes, J. Atmos. Sci., 56, 127–150, 1999.

Brunner, D., Staehelin, J., Rogers, H. L., Köhler, M. O., Pyle, J. A., Hauglustaine, D., Jourdain, L., Berntsen, T. K., Gauss, M., Isaksen, I. S. A., Meijer, E., van Velthoven, P., Pitari, G., Mancini, E., Grewe, G., and Sausen, R.: An evaluation of the performance of chemistry transport models by comparison with research aircraft observations. Part 1: Concepts and overall model performance, Atmos. Chem. Phys., 3, 1609–1631, doi:10.5194/acp-3-1609-2003, 2003.

Callies, J., Corpaccioli, E., Eisinger, M., Hahne, A., and Lefebvre, A.: GOME-2 Metop's Second-Generation Sensor for Operational Ozone Monitoring, ESA Bull., 102, 28–36, 2000.

Cammas, J.-P., Gilles, A., Chabrillat, S., Daerden, F., Elguindi, N., Flemming, J., Flentje, H., Deshler, C., T., Mercer, J. L., Smit, H. G. J., Stubi, R., Levrat, G., Johnson, B. J., Oltmans, S. J., Kivi, R., Thompson, A. M., Witte, J., Davies, J., Schmidlin, F. J., Brothers, G., and Sasaki, T.: Atmospheric comparison of electrochemical cell ozonesondes from different maufacturers, and with different cathode solution strengths: the Balloon Experiment on Standards for Ozonsondes, J. Geophys. Res., 113, D04307, doi:10.1029/2007JD008975, 2008.

Cape, J. N.: Surface ozone concentrations and ecosystem health: past trends and a guide to future projections, Sci. Total Environ., 400, 257–269, doi:10.1016/j.scitotenv.2008.06.025, 2008.





Clarisse, L., R'Honi, Y., Coheur, P.-F., Hurtmans, D., and Clerbaux, C.: Thermal infrared nadir observations of 24 atmospheric gases, Geophys. Res. Lett., 38, L10802, doi:10.1029/2011GL047271, 2011.

Clerbaux, C., Boynard, A., Clarisse, L., George, M., Hadji-Lazaro, J., Herbin, H., Hurtmans, D., Pommier, M., Razavi, A., Turquety, S., Wespes, C., and Coheur, P.-F.: Monitoring of atmospheric composition using the thermal infrared IASI/MetOp sounder, Atmos. Chem. Phys., 9, 6041–6054, doi:10.5194/acp-9-6041-2009, 2009.

Cooper, O. R., Parrish, D. D., Ziemke, J., Balashov, N. V., Cupeiro, M., Galbally, I. E., Gilge, S., Horowitz, L., Jensen, N. R., Lamarque, J.-F., Naik, V., Oltmans, S. J., Schwab, J., Shindell, D. T., Thompson, A. M., Thouret, V., Wang, Y., and Zbinden, R. M.: Global distribution and trends of tropospheric ozone: an observation-based review, Elem. Sci. Anth., 2, 10000029, doi:10.12952/journal.elementa.000029, 2014.

Cuevas, E., Camino, C., Benedetti, A., Basart, S., Terradellas, E., Baldasano, J. M., Morcrette, J.-J., Marticorena, B., Goloub, P., Mortier, A., Berjón, A., Hernández, Y., Gil-Ojeda, M., and Schulz, M.: The MACC-II 2007–2008 reanalysis: atmospheric dust evaluation and characterization over Northern Africa and Middle East, Atmos. Chem. Phys. Discuss., 14, 27797–27879, doi:10.5194/acpd-14-27797-2014, 2014.

Deeter, M. N., Emmons, L. K., Edwards, D. P., Gille, J. C., and Drummond, J. R.: Vertical resolution and information content of CO profiles retrieved by MOPITT, Geophys. Res. Lett., 31, L15112, doi:10.1029/2004GL020235, 2004.

Deeter, M., Edwards, D. P., Gille, J. C., Emmons, L., Francis, G. L., Ho, S.-P., Mao, D. Y., Worden, H. M., Drummond, J. R., and Novelli, P. C.: The MOPITT version 4 CO product: algorithm enhancements, validation, and long-term stability, J. Geophys. Res., 115, D07306, doi:10.1029/2009JD013005, 2010.

Deeter, M. N., Worden, H. M., Edwards, D. P., Gille, J. C., Mao, D., and Drummond, J. R.: MOPITT multispectral CO retrievals: ori-gins and effects of geophysical radiance errors, J. Geophys. Res., 116, D15303, doi:10.1029/2011JD015703, 2011.

Deeter, M. N., Worden, H. M., Edwards, D. P., Gille, J. C., and Andrews, A. E.: evaluation of MOPITT retrievals of lower-tropospheric carbon monoxide over the United States, J. Geophys. Res., 117, D13306, doi:10.1029/2012JD017553, 2012.

Deeter, M. N., Martínez-Alonso, S., Edwards, D. P., Emmons, L. K., Gille, J. C., Worden, H. M., Pittman, J. V., Daube, B. C., and Wofsy, S. C.: Validation of MOPITT Version 5 thermal-

infrared, near-infrared, and multispectral carbon monoxide profile retrievals for 2000–2011, J. Geophys. Res. Atmos., 118, 6710–6725, doi:10.1002/jgrd.50272, 2013.

De Wachter, E., Barret, B., Le Flochmoën, E., Pavelin, E., Matricardi, M., Clerbaux, C., Hadji-Lazaro, J., George, M., Hurtmans, D., Coheur, P.-F., Nedelec, P., and Cammas, J. P.: Retrieval of MetOp-A/IASI CO profiles and validation with MOZAIC data, Atmos. Meas. Tech., 5, 2843–2857, doi:10.5194/amt-5-2843-2012, 2012.

Drummond, J. R. and Mand, G. S.: The measurements of pollution in the troposphere (MOPITT) instrument: overall performance and calibration requirements, J. Atmos. Ocean. Technol., 13, 314–320, 1996.

Elguindi, N., Clark, H., Ordóñez, C., Thouret, V., Flemming, J., Stein, O., Huijnen, V., Moinat, P., Inness, A., Peuch, V.-H., Stohl, A., Turquety, S., Athier, G., Cammas, J.-P., and Schultz, M.: Current status of the ability of the GEMS/MACC models to reproduce the tropospheric CO vertical distribution as measured by MOZAIC, Geosci. Model Dev., 3, 501–518, doi:10.5194/gmd-3-501-2010, 2010.

Emmons, L. K., Edwards, D. P., Deeter, M. N., Gille, J. C., Campos, T., Nédélec, P., Novelli, P., and Sachse, G.: Measurements of Pollution In The Troposphere (MOPITT) validation through 2006, Atmos. Chem. Phys., 9, 1795–1803, doi:10.5194/acp-9-1795-2009, 2009.

Engelen, R. J., Serrar, S., and Chevallier, F.: Four-dimensional data assimilation of atmospheric $CO_2$ using AIRS observations, J. Geophys. Res., 114, D03303, doi:10.1029/2008JD010739, 2009.

Flemming, J. and Inness, A., Volcanic sulfur dioxide plume forecasts based on UV satellite retrievals for the 2011 Grímsvötn and the 2010 Eyjafjallajökull eruption, J. Geophys. Res.-Atmos., 118, 10172–10189, doi:10.1002/jgrd.50753, 2013.

Flemming, J., Inness, A., Flentje, H., Huijnen, V., Moinat, P., Schultz, M. G., and Stein, O.: Coupling global chemistry transport models to ECMWF's integrated forecast system, Geosci. Model Dev., 2, 253–265, doi:10.5194/gmd-2-253-2009, 2009.

Forster, P., Ramaswamy, V., Artaxo, P., Berntsen, T., Betts, R., Fahey, D. W., Haywood, J., Lean, J., Lowe, D. C., Myhre, G., Nganga, J., Prinn, R., Raga, G., Schulz, M., and Van Dorland, R.: Changes in Atmospheric Constituents and in Radiative Forcing in: Climate Change 2007: The Physical Science Basis. Contribution of Working Group I to the Fourth Assessment Report of the Intergovernmental Panel on Climate Change, edited by: Solomon, S., Qin, D., Manning, M., Chen, Z., Marquis, M., Averyt, K. B., Tignor, M., and Miller, H. L., USA, 2007.





George, M., Clerbaux, C., Hurtmans, D., Turquety, S., Coheur, P.-F., Pommier, M., Hadji-Lazaro, J., Edwards, D. P., Worden, H., Luo, M., Rinsland, C., and McMillan, W.: Carbon monoxide distributions from the IASI/METOP mission: evaluation with other space-borne remote sensors, Atmos. Chem. Phys., 9, 8317–8330, doi:10.5194/acp-9-8317-2009, 2009.

George, M., Clerbaux, C., Bouarar, I., Coheur, P.-F., Deeter, M. N., Edwards, D. P., Francis, G., Gille, C., Hadji-Lazaro, J., Hurtmans, D., Inness, A., Mao, D., and Worden H. M.: An examination of the long-term CO records from MOPITT and IASI and comparison of retrieval methodology, Atmos. Meas. Tech. Discuss., submitted, 2015.

Gomez-Pelaez, A. J., Ramos, R., Gomez-Trueba, V., Novelli, P. C., and Campo-Hernandez, R.: A statistical approach to quantify uncertainty in carbon monoxide measurements at the Izaña global GAW station: 2008–2011, Atmos. Meas. Tech., 6, 787–799, doi:10.5194/amt-6-787-2013, 2013.

Granier, C., Huijnen, V., Inness, A., Jones, L., Katragkou, E., Khokhar, F., Kins, L., Law, K., Lefever, K., Leitao, J., Melas, D., Moinat, P., Ordonez, C., Peuch, V.-H., Reich, G., Schultz, M., Stein, O., Thouret, V., Werner, T., and Zerefos, C.: GEMS GRG Comprehensive Validation Report, available as project report at: http://gems.ecmwf.int (last access: February 2015), 2009.

Granier, C., Bessagnet, B., Bond, T., D'Angiola, A., van der Gon, H. D., Frost, G. J., Heil, A., Kaiser, J. W., Kinne, S., Klimont, Z., Kloster, S., Lamarque, J.-F., Liousse, C., Masui, T., Meleux, F., Mieville, A., Ohara, T., Raut, J. C., Riahi, K., Schultz, M. G., Smith, S. J., Thompson, A., van Aardenne, J., van der Werf, G. R., and van Vuuren, D. P.: Evolution of anthropogenic and biomass burning emissions of air pollutants at global and regional scales during the 1980–2010 period, Climatic Change, 109, 163–190, doi:10.1007/s10584-011-0154-1, 2011.

Griffin, R. J., Chen, J., Carmody, K., and Vutukuru, S.: Contribution of gas phase oxidation of volatile organic compounds to atmospheric carbon monoxide levels in two areas of the united States, J. Geophys. Res., 11, D10S17, doi:10.1029/2006JD007602, 2007.

Guenther, A., Karl, T., Harley, P., Wiedinmyer, C., Palmer, P. I., and Geron, C.: Estimates of global terrestrial isoprene emissions using MEGAN (Model of Emissions of Gases and Aerosols from Nature), Atmos. Chem. Phys., 6, 3181–3210, doi:10.5194/acp-6-3181-2006, 2006.

He, Y., Uno, I., Wang, Z., Ohara, T., Sugimoto, N., Shimizu, A., Richter, A., and Burrows, J. P.: Variations of the increasing trend of tropospheric $NO_2$ over central east China during the past decade, Atmos. Environ., 41, 4865–4876, 2007.

Hilboll, A., Richter, A., and Burrows, J. P.: Long-term changes of tropospheric $NO_2$ over megacities derived from multiple satellite instruments, Atmos. Chem. Phys., 13, 4145–4169, doi:10.5194/acp-13-4145-2013, 2013a.

Hilboll, A., Richter, A., Rozanov, A., Hodnebrog, Ø., Heckel, A., Solberg, S., Stordal, F., and Burrows, J. P.: Improvements to the retrieval of tropospheric $NO_2$ from satellite – stratospheric correction using SCIAMACHY limb/nadir matching and comparison to Oslo CTM2 simulations, Atmos. Meas. Tech., 6, 565–584, doi:10.5194/amt-6-565-2013, 2013b.

Hollingsworth, A., Engelen, R. J., Benedetti, A., Dethof, A., Flemming, J., Kaiser, J. W., and Simmons, A. J.: Toward a monitoring and forecasting system for atmospheric composition: the GEMS project, B. Am. Meteorol. Soc., 89, 1147–1164, doi:10.1175/2008BAMS2355.1, 2008.

Hudman, R. C., Murray, L. T., Jacob, D. J., Millet, D. B., Turquety, S., Wu, S., Blake, D. R., Goldstein, A. H., Holloway, J., and Sachse, G. W.: Biogenic versus anthropogenic sources of CO over the United States, Geophys. Res. Lett., 35, L04801, doi:10.1029/2007GL032393, 2008.

Huijnen, V., Williams, J., van Weele, M., van Noije, T., Krol, M., Dentener, F., Segers, A., Houweling, S., Peters, W., de Laat, J., Boersma, F., Bergamaschi, P., van Velthoven, P., Le Sager, P., Eskes, H., Alkemade, F., Scheele, R., Nédélec, P., and Pätz, H.-W.: The global chemistry transport model TM5: description and evaluation of the tropospheric chemistry version 3.0, Geosci. Model Dev., 3, 445–473, doi:10.5194/gmd-3-445-2010, 2010.

Huijnen, V., Flemming, J., Kaiser, J. W., Inness, A., Leitão, J., Heil, A., Eskes, H. J., Schultz, M. G., Benedetti, A., Hadji-Lazaro, J., Dufour, G., and Eremenko, M.: Hindcast experiments of tropospheric composition during the summer 2010 fires over western Russia, Atmos. Chem. Phys., 12, 4341–4364, doi:10.5194/acp-12-4341-2012, 2012.

Hurtmans, D., Coheur, P.-F., Wespes, C., Clarisse, L., Scharf, O., Clerbaux, C., Hadji-Lazaro, J., George, M., and Turquety, S.: FORLI radiative transfer and retrieval code for IASI, J. Quant. Spectrosc. Radiat. T., 113, 1391–1408, doi:10.1016/j.jqsrt.2012.02.036, 2012.

Inness, A., Flemming, J., Suttie, M., and Jones, L.: GEMS data assimilation system for chemically reactive gases. ECMWF RD Tech Memo 587, available at: http://www.ecmwf.int (last access: February 2015), 2009.





Inness, A., Baier, F., Benedetti, A., Bouarar, I., Chabrillat, S., Clark, H., Clerbaux, C., Coheur, P., Engelen, R. J., Errera, Q., Flemming, J., George, M., Granier, C., Hadji-Lazaro, J., Huijnen, V., Hurtmans, D., Jones, L., Kaiser, J. W., Kapsomenakis, J., Lefever, K., Leitão, J., Razinger, M., Richter, A., Schultz, M. G., Simmons, A. J., Suttie, M., Stein, O., Thépaut, J.-N., Thouret, V., Vrekoussis, M., Zerefos, C., and the MACC team: The MACC reanalysis: an 8 yr data set of atmospheric composition, Atmos. Chem. Phys., 13, 4073–4109, doi:10.5194/acp-13-4073-2013, 2013.

Itahashi, S., Uno, I., Irie, H., Kurokawa, J.-I., and Ohara, T.: Regional modeling of tropospheric $NO_2$ vertical column density over East Asia during the period 2000–2010: comparison with multisatellite observations, Atmos. Chem. Phys., 14, 3623–3635, doi:10.5194/acp-14-3623-2014, 2014.

Kaiser, J. W., Heil, A., Andreae, M. O., Benedetti, A., Chubarova, N., Jones, L., Morcrette, J.-J., Razinger, M., Schultz, M. G., Suttie, M., and van der Werf, G. R.: Biomass burning emissions estimated with a global fire assimilation system based on observed fire radiative power, Biogeosciences, 9, 527–554, doi:10.5194/bg-9-527-2012, 2012.

Kalnay, E.: Atmospheric Modeling, Data Assimilation and Predictability, Cambridge University Press, Cambridge, 2003.

Kalnay, E., Kanamitsu, M., Kistler, R., Collins, W., Deaven, D., Gandin, L., Iredell, M., Saha, S., White, G., Woollen, J., Zhu, Y., Chelliah, M., Ebisuzaki, W., Higgins, W., Janowiak, J., Mo, K. C., Ropelewski, C., Wang, J., Leetmaa, A., Reynolds, R., Jenne, R., and Joseph, D.: The NCEP/NCAR 40-Year Reanalysis Project, B. Am. Meteorol. Soc., 77, 437–471, doi:10.1175/1520-0477(1996)077<0437:TNYRP>2.0.CO;2, 1996.

Kerzenmacher, T., Dils, B., Kumps, N., Blumenstock, T., Clerbaux, C., Coheur, P.-F., Demoulin, P., García, O., George, M., Griffith, D. W. T., Hase, F., Hadji-Lazaro, J., Hurtmans, D., Jones, N., Mahieu, E., Notholt, J., Paton-Walsh, C., Raffalski, U., Ridder, T., Schneider, M., Servais, C., and De Mazière, M.: Validation of IASI FORLI carbon monoxide retrievals using FTIR data from NDACC, Atmos. Meas. Tech., 5, 2751–2761, doi:10.5194/amt-5-2751-2012, 2012.

Kinnison, D. E., Brasseur, G. P., Walters, S., Gracia, R. R., Marsh, D. R., Sassi, F., Harvey, V. L., Randall, C. E., Emmons, L., Lamarque, J. F., Hess, P., Orlando, J. J., Tie, X. X., Randel, W., Pan, L. L., Gettelman, A., Granier, C., Diehl, T., Niemeier, U., and Simmons, A. J.: Sensitivity of chemical tracers to meteorological parameters in the MOZART-3 chemical transport model, J. Geophys. Res, 112, D20302, doi:10.1029/2006JD007879, 2007.

Lefever, K., van der A, R., Baier, F., Christophe, Y., Errera, Q., Eskes, H., Flemming, J., Inness, A., Jones, L., Lambert, J.-C., Langerock, B., Schultz, M. G., Stein, O., Wagner, A., and Chabrillat, S.: Copernicus atmospheric service for stratospheric ozone: validation and intercomparison of four near real-time analyses, 2009–2012, Atmos. Chem. Phys. Discuss., 14, 12461–12523, doi:10.5194/acpd-14-12461-2014, 2014.

Leitão, J., Richter, A., Vrekoussis, M., Kokhanovsky, A., Zhang, Q. J., Beekmann, M., and Burrows, J. P.: On the improvement of $NO_2$ satellite retrievals – aerosol impact on the airmass factors, Atmos. Meas. Tech., 3, 475–493, doi:10.5194/amt-3-475-2010, 2010.

Leue, C., Wenig, M., Wagner, T., Platt, U., and Jähne, B.: Quantitative analysis of NOx emissions from GOME satellite image sequences, J. Geophys. Res., 106, 5493–5505, 2001.

Massart, S., Agusti-Panareda, A., Aben, I., Butz, A., Chevallier, F., Crevoisier, C., Engelen, R., Frankenberg, C., and Hasekamp, O.: Assimilation of atmospheric methane products into the MACC-II system: from SCIAMACHY to TANSO and IASI, Atmos. Chem. Phys., 14, 6139–6158, doi:10.5194/acp-14-6139-2014, 2014.

Mohnen, V. A., Goldstein, and Wang, W.-C.: Tropospheric ozone and climate change, Air Waste Manage., 43, 1332–1334, doi:10.1080/1073161X.1993.10467207, 1993.

Morcrette, J.-J., Boucher, O., Jones, L., Salmond, D., Bechthold, P., Beljaars, A., Benedetti, A., Bonet, A., Kaiser, J. W., Razinger, M., Schulz, M., Serrar, S., Simmons, A. J., Sofiev, M., Suttie, M., Tompkins, A. M., and Untch, A.: Aerosol analysis and forecast in the European Centre for Medium-Range Weather Forecasts Integrated Forecast System: forward modeling, J. Geophys. Res., 114, D06206, doi:10.1029/2008JD011235, 2009.

Naik, V., Voulgarakis, A., Fiore, A. M., Horowitz, L. W., Lamarque, J.-F., Lin, M., Prather, M. J., Young, P. J., Bergmann, D., Cameron-Smith, P. J., Cionni, I., Collins, W. J., Dalsøren, S. B., Doherty, R., Eyring, V., Faluvegi, G., Folberth, G. A., Josse, B., Lee, Y. H., MacKenzie, I. A., Nagashima, T., van Noije, T. P. C., Plummer, D. A., Righi, M., Rumbold, S. T., Skeie, R., Shindell, D. T., Stevenson, D. S., Strode, S., Sudo, K., Szopa, S., and Zeng, G.: Preindustrial to present-day changes in tropospheric hydroxyl radical and methane lifetime from the Atmospheric Chemistry and Climate Model Intercomparison Project (ACCMIP), Atmos. Chem. Phys., 13, 5277–5298, doi:10.5194/acp-13-5277-2013, 2013.

Novelli, P. C., Masarie, K. A., and Lang, P. M.: Distributions and recent changes of carbon monoxide in the lower troposphere, J. Geophys. Res., 103, 19015–19033, doi:10.1029/98JD01366, 1998.





Ordóñez, C., Elguindi, N., Stein, O., Huijnen, V., Flemming, J., Inness, A., Flentje, H., Katragkou, E., Moinat, P., Peuch, V.-H., Segers, A., Thouret, V., Athier, G., van Weele, M., Zerefos, C. S., Cammas, J.-P., and Schultz, M. G.: Global model simulations of air pollution during the 2003 European heat wave, Atmos. Chem. Phys., 10, 789–815, doi:10.5194/acp-10-789-2010, 2010.

Park, R. J., Pickering, K. E., Allen, D. J., Stenchikov, G. L., and Fox-Rabinovitz, M. S.: Global simulation of tropospheric ozone using the University of Maryland Chemical Transport Model (UMD-CTM): 1. Model description and evaluation, J. Geophys. Res., 109, D09301, doi:10.1029/2003JD004266, 2004.

Penkett, S., Gilge, S., Plass-Duelmer, C., and Galbally, I.: WMO/GAW Expert Workshop on Global Long-term Measurements of Nitrogen Oxides and Recommendations for GAW Nitrogen Oxides Network, WMO, Geneva, 2011.

Platt, U. and Stutz, J.: Differential Optical Absorption Spectroscopy. Physics of Earth and Space Environments, Springer, Berlin, available at: http://www.springerlink.com/content/978-3-540-21193-8 (last access: February 2015), 2008.

Richter, A. and Burrows, J. P.: Tropospheric $NO_2$ from GOME measurements, Adv. Space Res., 29, 1673–1683, doi:10.1016/S0273-1177(02)00100-X, 2002.

Richter, A., Burrows, J. P., Nüß, H., Granier, C., and Niemeier, U.: Increase in tropospheric nitrogen dioxide over China observed from space, Nature, 437, 129–132, doi:10.1038/nature04092, 2005.

Richter, A., Begoin, M., Hilboll, A., and Burrows, J. P.: An improved $NO_2$ retrieval for the GOME-2 satellite instrument, Atmos. Meas. Tech., 4, 1147–1159, doi:10.5194/amt-4-1147-2011, 2011.

Rodgers, C. D.: Inverse Methods for Atmospheric Sounding, Theory and Practice, World Scientific, Singapore, 2000.

Rozanov, A., Vladimir, V., Rozanov, M., Buchwitz, A., Kokhanovsky, A., and Burrows, J. P.: SCIATRAN 2.0 – a new radiative transfer model for geophysical applications in the 175–2400 Nm spectral region, Adv. Space Res., 36, 1015–1019, doi:10.1016/j.asr.2005.03.012, 2005.

Santer, B. D., Sausen, R., Wigley, T. M. L., Boyle, J. S., AchutaRao, K., Doutriaux, C., Hansen, J. E., Meehl, G. A., Roeckner, E., Ruedy, R., Schmidt, G., and Taylor, K. E.: Behavior of tropopause height and atmospheric temperature in models, reanalyses, and observations: decadal changes, J. Geophys. Res., 108, 4002, doi:10.1029/2002JD002258, 2003.

Schaap, M., Renske, M. A., Timmermans, M. R., Boersen, G. A. C., and Builtjes, P. J. H.: The LOTOS-EUROS model: description, validation and latest developments, Int. J. Environ. Pollut., 32, 270–290, 2008.

Schreier, S. F., Richter, A., Kaiser, J. W., and Burrows, J. P.: The empirical relationship between satellite-derived tropospheric $NO_2$ and fire radiative power and possible implications for fire emission rates of $NO_x$, Atmos. Chem. Phys., 14, 2447–2466, doi:10.5194/acp-14-2447-2014, 2014.

Schultz, M. G., Backman, L., Balkanski, Y., Bjoerndalsaeter, S., Brand, R., Burrows, J. P., Dalsoeren, S., de Vasconcelos, M., Grodtmann, B., Hauglustaine, D. A., Heil, A., Hoelzemann, J. J., Isaksen, I. S. A., Kaurola, J., Knorr, W., Ladstaetter-Weißenmayer, B., Mota, A., Oom, D., Pacyna, J., Panasiuk, D., Pereira, J. M. C., Pulles, T., Pyle, J., Rast, S., Richter, A., Savage, N., Schnadt, C., Schulz, M., Spessa, A., Staehelin, J., Sundet, J. K., Szopa, S., Thonicke, K., van het, Bolscher, M., van Noije, T., van Velthoven, P., Vik, A. F., and Wittrock, F.: REanalysis of the TROpospheric chemical composition over the past 40 years (RETRO) – A long-term global modeling study of tropospheric chemistry, Final Report Jülich/Hamburg, Germany, published as report no. 48/2007 in the series "Reports on Earth System Science" of the Max Planck Institute for Meteorology, Hamburg, ISSN 1614-1199, 2007.

Selin, N. E., Wu, S., Reilly, J. M., Paltsev, S., Prinn, R. G., and Webster, M. D.: Global health and economic impacts of future ozone pollution, Environ. Res. Lett., 4, 044014, doi:10.1088/1748-9326/4/4/044014, 2009.

Shindell, D. T., Faluvegi, G., Stevenson, D. S., Krol, M. C., Emmons, L. K., Lamarque, J.-F., Pétron, G., Dentener, F. J., Ellingsen, K., Schultz, M. G., Wild, O., Amann, M., Atherton, C. S., Bergmann, D. J., Bey, I., Butler, T., Cofala, J., Collins, W. J., Derwent, R. G., Doherty, R. M., Drevet, J., Eskes, H. J., Fiore, A. M., Gauss, M., Hauglustaine, D. A., Horowitz, L. W., Isaksen, I. S. A., Lawrence, M. G., Montanaro, V., Müller, J.-F., Pitari, G., Prather, M. J., Pyle, J. A., Rast, S., Rodriguez, J. M., Sanderson, M. G., Savage, N. H., Strahan, S. E., Sudo, K., Szopa, S., Unger, N., van Noije, T. P. C., and Zeng, G.: Multi-model simulations of carbon monoxide: comparison with observations and projected near-future changes, J. Geophys. Res., 111, D19306, doi:10.1029/2006JD007100, 2006.

Seinfeld, J. H. and Pandis, S. N.: Atmospheric Chemistry and Physics: From Air Pollution to Climate Change, John Wiley, Hoboken, NJ, 2006.





Sinnhuber, B. M., Weber, M., Amankwah, A., and Burrows, J. P.: Total Ozone during the Unusual Antarctic Winter of 2002, Geophys. Res. Lett., 30, 1580–1584, doi:10.1029/2002GL016798, 2003.

Sinnhuber, M., Burrows, J. P., Chipperfield, M. P., Jackman, C. H., Kallenrode, M.-B., Künzi, K. F., and Quack, M.: A model study of the impact of magnetic field structure on atmospheric composition during solar proton events, Geophys. Res. Lett., 30, 1818–1821, doi:10.1029/2003GL017265, 2003.

Stein, O., Schultz, M. G., Flemming, J., Inness, A., Kaiser, J., Jones, L., Benedetti, A., Morcrette, J.-J.: MACC Global air quality services – Technical Documentation. MACC project deliverable D_G-RG_3.8, available at: http://www.gmes-atmosphere.eu/documents/deliverables/g-rg/ (last access: February 2015), 2011.

Stein, O., Flemming, J., Inness, A., Kaiser, J. W., and Schultz, M. G.: Global reactive gases and reanalysis in the 5 MACC project, J. Integr. Environ. Sci., 9, 57–70, doi:10.1080/1943815X.2012.696545, 2012.

Stein, O., Huijnen, V., Flemming, J.: Model description of the IFS-MOZART and IFS-TM5 coupled systems. MACC-II project deliverable D_55.4, available at: https://www.gmes-atmosphere.eu/documents/maccii/deliverables/grg/ (last access: February 2015), 2013.

Stein, O., Schultz, M. G., Bouarar, I., Clark, H., Huijnen, V., Gaudel, A., George, M., and Clerbaux, C.: On the wintertime low bias of Northern Hemisphere carbon monoxide found in global model simulations, Atmos. Chem. Phys., 14, 9295–9316, doi:10.5194/acp-14-9295-2014, 2014.

Tørseth, K., Aas, W., Breivik, K., Fjæraa, A. M., Fiebig, M., Hjellbrekke, A. G., Lund Myhre, C., Solberg, S., and Yttri, K. E.: Introduction to the European Monitoring and Evaluation Programme (EMEP) and observed atmospheric composition change during 1972–2009, Atmos. Chem. Phys., 12, 5447–5481, doi:10.5194/acp-12-5447-2012, 2012.

Valcke, S., Redler, R.: OASIS4 User Guide (OASIS4_0_2). PRISM-Support Initiative, Technical Report No 4, available at: http://www.prism.enes.org/Publications/Reports/OASIS4_User_Guide_T4.pdf (last access: February 2015), 2006.

Val Martin, M., Heald, C. L., and Arnold, S. R.: Coupling dry deposition to vegetation phenology in the Community Earth System Model: implications for the simulation of surface $O_3$, Geophys. Res. Lett., 41, 2988–2996, doi:10.1002/2014GL059651, 2014.

van der Werf, G. R., Randerson, J. T., Giglio, L., Collatz, G. J., Kasibhatla, P. S., and Arellano Jr., A. F.: Interannual variability in global biomass burning emissions from 1997 to 2004, Atmos. Chem. Phys., 6, 3423–3441, doi:10.5194/acp-6-3423-2006, 2006.

Velders, G. J. M., Granier, C., Portmann, R. W., Pfeilsticker, K., Wenig, M., Wagner, T., Platt, U., Richter, A., and Burrows, J. P.: Global tropospheric $NO_2$ column distributions: comparing 3-D model calculations with GOME measurements, J. Geophys. Res., 106, 12643–12660, 2001.

Wang, P., Stammes, P., van der A, R., Pinardi, G., and van Roozendael, M.: FRESCO+: an improved $O_2$ A-band cloud retrieval algorithm for tropospheric trace gas retrievals, Atmos. Chem. Phys., 8, 6565–6576, doi:10.5194/acp-8-6565-2008, 2008.

Winkler, H., Sinnhuber, M., Notholt, J., Kallenrode, M. B., Steinhilber, F., Vogt, J., Zieger, B., Glassmeier, K. H., and Stadelmann, A.: Modeling impacts of geomagnetic field variations on middle atmospheric ozone responses to solar proton events on long timescales, J. Geophys. Res., 113, D02302, doi:10.1029/2007JD008574, 2008.

WMO: WMO Global Atmosphere Watch (GAW) Strategic Plan: 2008–2015, World Meteorological Organization, Geneva, Switzerland, 2007a.

WMO: Guidelines for the Measurement of Atmospheric Carbon Monoxide, GAW Report No. 192, World Meteorological Organization, Geneva, Switzerland, 2007b.

WMO: 16th WMO/IAEA Meeting on Carbon Dioxide, Other greenhouse Gases and Related Measurement Techniques (GGMT-2011), Geneva, 2012.

WMO: Guidelines for the Continuous Measurements of Ozone in the Troposphere, GAW Report No. 209, World Meteorological Organization, Geneva, Switzerland, 2013.

Worden, H. M., Deeter, M. N., Edwards, D. P., Gille, J. C., Drummond, J. R., and Nedelec, P. P.: Observations of near-surface carbon monoxide from space using MOPITT multispectral retrievals, J. Geophys. Res., 115, D18314, doi:10.1029/2010JD014242, 2010.

Worden, H. M., Deeter, M. N., Edwards, D. P., Gille, J., Drummond, J., Emmons, L. K., Francis, G., Martínez-Alonso, S.: 13 years of MOPITT operations: lessons from MOPITT retrieval algorithm development, Ann. Geophys., 56, doi:10.4401/ag-6330, 2014.





**Table 1.** Description of the set-up of the MACC_osuite between September 2009 and December 2012. Details on the assimilated data are provided in Table 2. A description of the emissions is given in Sect. 2.1.1 in the text.

| Model Cycle | CTM | Assimilated Data | Emissions |
|---|---|---|---|
| CY36R1 | MOZART v3.0 | $O_3$ (MLS, OMI, SBUV-2 SCIAMACHY), CO (IASI) | RETRO/REAS/GEIA/GFEDv2/GFAS |
| CY37R3 | MOZART v3.5 | $O_3$ (MLS, OMI, SBUV-2), CO (IASI, MOPITT), $NO_2$ (OMI), $SO_2$ (OMI) | MACCity/MEGAN/GFASv1.0 daily |

**Table 2.** List of assimilated data in the MACC_osuite.

| Instrument | Satellite | Provider | Version | Type | Status |
|---|---|---|---|---|---|
| MLS | AURA | NASA | V02 | $O_3$ Profiles | 1 Sep 2009–31 Dec 2012 |
| OMI | AURA | NASA | V883 | $O_3$ Total column | 1 Sep 2009–31 Dec 2012 |
| SBUV-2 | NOAA | NOAA | V8 | $O_3$ 6 layer profiles | 1 Sep 2009–31 Dec 2012 |
| SCIAMACHY | Envisat | KNMI | | $O_3$ total column | 16 Sep 2009–8 Apr 2012 |
| IASI | MetOp-A | LATMOS/ ULB | | CO Total column | 1 Sep 2009–31 Dec 2012 |
| MOPITT | TERRA | NCAR | V4 | CO Total column | 5 Jul 2012–31 Dec 2012 |
| OMI | AURA | KNMI | DOMINO V2.0 | $NO_2$ Tropospheric column | 5 Jul 2012–31 Dec 2012 |
| OMI | AURA | NASA | v003 | $SO_2$ Tropospheric column | 5 Jul 2012–31 Dec 2012 |
| MODIS | AQUA/ TERRA | NASA | Col. 5 | Aerosol total optical depth | 1 Sep 2009–31 Dec 2012 |



**Table 3.** List of GAW and EMEP stations used in the evaluation.

| Station | Label/ Region | Programme | Lat | Lon | Alt [m a.s.l.] | Station | Label/ Region | Programme | Lat | Lon | Alt [m a.s.l.] |
|---|---|---|---|---|---|---|---|---|---|---|---|
| Ähtäri II | NE | EMEP | 62.58 | 24.18 | 180 | Masenberg | CE | EMEP | 47.35 | 15.88 | 1170 |
| Alert | ALT | GAW | 82.45 | −62.52 | 210 | Mauna Loa | MAU | GAW | 19.54 | −155.58 | 3397 |
| Arrival Heights | ARH | GAW | −77.80 | 166.67 | 184 | Minamitorishima | MNM | GAW | 24.29 | 153.98 | 8 |
| Aspvreten | NE | EMEP | 58.80 | 17.38 | 20 | Montandon | CE | EMEP | 47.30 | 6.83 | 836 |
| Assekrem | ASS | GAW | 23.27 | 5.63 | 2710 | Monte Cimone | MCI | GAW | 44.18 | 10.70 | 2165 |
| Aston Hill | NE | EMEP | 52.50 | −3.03 | 370 | Monte Velho | SE | EMEP | 38.08 | −8.80 | 43 |
| Auchencorth | NE | EMEP | 55.79 | −3.24 | 260 | Montelibretti | CE | EMEP | 42.10 | 12.63 | 48 |
| Ayia Marina | SE | EMEP | 35.04 | 33.06 | 532 | Montfranc | CE | EMEP | 45.80 | 2.07 | 810 |
| Barcarrola | SE | EMEP | 38.47 | −6.92 | 393 | Morvan | CE | EMEP | 47.27 | 4.08 | 620 |
| Baring Head | BAH | GAW | −41.41 | 174.87 | 85 | Narberth | NE | EMEP | 51.23 | −4.70 | 160 |
| Barrow | BAR | GAW | 71.32 | −156.60 | 11 | Neuglobsow | NGW/NE | GAW/EMEP | 53.17 | 13.03 | 62 |
| BEO Moussala | BEO | GAW | 42.18 | 23.59 | 2925 | Neumayer | NEU | GAW | −70.65 | −8.25 | 42 |
| Birkenes | NE | EMEP | 58.38 | 8.25 | 190 | Niembro | CE | EMEP | 43.44 | −4.85 | 134 |
| Bredkälen | NE | EMEP | 63.85 | 15.33 | 404 | Norra-Kvill | NE | EMEP | 57.81 | 15.56 | 261 |
| Bush | NE | EMEP | 55.86 | −3.21 | 180 | O Saviñao | CE | EMEP | 43.23 | −7.70 | 506 |
| Cabauw | NE | EMEP | 51.97 | 4.92 | 60 | Offagne | CE | EMEP | 49.88 | 5.20 | 430 |
| Cabo de Creus | CE | EMEP | 42.32 | 3.32 | 23 | Oulanka | NE | EMEP | 66.32 | 29.40 | 310 |
| Cairo | CAI | GAW | 30.08 | 31.28 | 35 | Pallas | NE | EMEP | 68.00 | 24.15 | 340 |
| Campisabalos | CE | EMEP | 41.28 | −3.14 | 1360 | Payerne | PAY/CE | GAW/EMEP | 46.81 | 6.94 | 510 |
| Cape Grim | CAG | GAW | −40.68 | 144.68 | 94 | Penausende | CE | EMEP | 41.28 | −5.86 | 985 |
| Cape Point | CAP | GAW | −34.35 | 18.48 | 230 | Peyrusse Vieille | CE | EMEP | 43.62 | 0.18 | 200 |
| Cape Verde | CVO | GAW | 16.85 | −24.87 | 10 | Pic du Midi | PIC/CE | GAW/EMEP | 42.94 | 0.14 | 2877 |
| Charlton Mackrell | NE | EMEP | 51.06 | −2.68 | 54 | Pillersdor | CE | EMEP | 48.72 | 15.94 | 315 |
| Chaumont | CE | EMEP | 47.05 | 6.98 | 1130 | Preila | NE | EMEP | 55.35 | 21.07 | 5 |
| Chibougamau | CHI | GAW | 49.68 | −74.34 | 393 | Prestebakke | NE | EMEP | 59.00 | 11.53 | 160 |
| Chopok | CE | EMEP | 48.93 | 19.58 | 2008 | Puy de Dôme | PUY/CE | GAW/EMEP | 45.77 | 2.95 | 1465 |
| Concordia | CON | GAW | −75.10 | 123.33 | 3233 | Ragged Point | RAG | GAW | 13.17 | −59.43 | 45 |
| De Zilk | NE | EMEP | 52.30 | 4.50 | 4 | Rao | NE | EMEP | 57.39 | 11.91 | 10 |
| Diabla Gora | NE | EMEP | 54.15 | 22.07 | 157 | Revin | CE | EMEP | 49.90 | 4.63 | 390 |
| Dobele | DOB | GAW | 56.37 | 23.19 | 42 | Rigi | RIG/CE | GAW/EMEP | 47.07 | 8.46 | 1030 |
| Doñana | SE | EMEP | 37.03 | −6.33 | 5 | Rojen Peak | CE | EMEP | 41.70 | 24.74 | 1750 |
| Donon | CE | EMEP | 48.50 | 7.13 | 775 | Rucava | RUC/NE | GAW/EMEP | 56.10 | 21.10 | 18 |
| Dunkelsteinerwald | CE | EMEP | 48.37 | 15.55 | 320 | Ryori | RYO | GAW | 39.03 | 141.82 | 260 |
| East Trout Lake | ETL | GAW | 54.35 | −104.98 | 492 | Sable Island | SAB | GAW | 43.93 | −60.02 | 5 |
| Egbert | EGB | GAW | 44.23 | −79.78 | 253 | San Pablo de los Montes | SE | EMEP | 39.55 | −4.35 | 917 |
| Eibergen | NE | EMEP | 52.08 | 6.57 | 20 | Sandve | NE | EMEP | 59.20 | 5.20 | 15 |
| Els Torms | CE | EMEP | 41.40 | 0.72 | 470 | Schauinsland | SCH/CE | GAW/EMEP | 47.92 | 7.92 | 1205 |
| Eskdalemuir | NE | EMEP | 55.31 | −3.20 | 243 | Schmücke | NE | EMEP | 50.65 | 10.77 | 937 |
| Esrange | NE | EMEP | 67.88 | 21.07 | 475 | Sibton | NE | EMEP | 52.29 | 1.46 | 46 |
| Estevan Point | ESP | GAW | 49.38 | −126.55 | 39 | Śnieżka | NE | EMEP | 50.73 | 15.73 | 1603 |
| Eupen | NE | EMEP | 51.46 | 6.00 | 295 | Sonnblick | SBL/CE | GAW/EMEP | 47.05 | 12.96 | 3106 |
| Everest-Pyramid | EVP | GAW | 27.96 | 86.82 | 5079 | South Pole | SPO | GAW | −89.98 | −24.80 | 2810 |
| Finokalia | SE | EMEP | 35.32 | 25.67 | 250 | Spitsbergen | NE | EMEP | 78.90 | 11.88 | 474 |
| Forsthof | CE | EMEP | 48.10 | 15.91 | 581 | St. Osyth | NE | EMEP | 51.78 | 1.08 | 8 |
| Fraserdale | FRA | GAW | 49.88 | −81.57 | 210 | Stará Lesná | CE | EMEP | 49.15 | 20.28 | 808 |
| Gänserndorf | CE | EMEP | 48.33 | 16.73 | 161 | Starina | CE | EMEP | 49.05 | 22.27 | 345 |
| Gerlitzen | CE | EMEP | 46.69 | 13.92 | 1895 | Stixneusiedl | CE | EMEP | 48.05 | 16.68 | 240 |

**Table 3.** Continued.

| Station | Label/ Region | Programme | Lat | Lon | Alt [m a.s.l.] | Station | Label/ Region | Programme | Lat | Lon | Alt [m a.s.l.] |
|---|---|---|---|---|---|---|---|---|---|---|---|
| Graz Platte | CE | EMEP | 47.11 | 15.47 | 651 | Strath Vaich Dam | NE | EMEP | 57.73 | −4.77 | 270 |
| Great Dun Fell | NE | EMEP | 54.68 | −2.45 | 847 | Summit | SUM | GAW | 72.58 | −38.48 | 3238 |
| Grebenzen | CE | EMEP | 47.04 | 14.33 | 1648 | Svratouch | CE | EMEP | 49.73 | 16.05 | 737 |
| Grimsoe | NE | EMEP | 59.73 | 15.47 | 132 | Syowa Station | SYO | GAW | −69.00 | 39.58 | 16 |
| Harwell | NE | EMEP | 51.57 | −1.32 | 137 | Tänikon | CE | EMEP | 47.48 | 8.90 | 540 |
| Haunsberg | CE | EMEP | 47.97 | 13.02 | 730 | Topolniky | CE | EMEP | 47.96 | 17.86 | 113 |
| Heidenreichstein | CE | EMEP | 48.88 | 15.05 | 570 | Trinidad Head | TRI | GAW | 41.05 | −124.15 | 120 |
| High Muffles | NE | EMEP | 54.33 | −0.80 | 267 | Tsukuba | TSU | GAW | 36.05 | 140.13 | 25 |
| Hurdal | NE | EMEP | 60.37 | 11.08 | 300 | Tudor Hill | TUD | GAW | 32.27 | −64.87 | 30 |
| Illmitz | CE | EMEP | 47.77 | 16.77 | 117 | Tustervatn | NE | EMEP | 65.83 | 13.92 | 439 |
| Iskrba | ISK/CE | GAW/EMEP | 45.56 | 14.86 | 520 | Tutuila | TUT | GAW | −14.24 | −170.57 | 42 |
| Izaña (Tenerife) | IZO | GAW | 28.30 | −16.50 | 2367 | Ushuaia | USH | GAW | −54.85 | −68.32 | 18 |
| Jarczew | NE | EMEP | 51.82 | 21.98 | 180 | Utö | NE | EMEP | 59.78 | 21.38 | 7 |
| Jungfraujoch | JFJ/CE | GAW/EMEP | 46.55 | 7.99 | 3578 | Vavihill | NE | EMEP | 56.01 | 13.15 | 175 |
| Karasjok | NE | EMEP | 69.47 | 25.22 | 333 | Vezin | NE | EMEP | 50.50 | 4.99 | 160 |
| Keldsnor | NE | EMEP | 54.73 | 10.73 | 10 | Vilsandi | NE | EMEP | 58.38 | 21.82 | 6 |
| Kollumerwaard | KOW/NE | GAW/EMEP | 53.33 | 6.28 | 1 | Vindeln | VIN/NE | GAW/EMEP | 64.25 | 19.77 | 225 |
| Košetice | KOS/CE | GAW/EMEP | 49.58 | 15.08 | 534 | Virolahti II | NE | EMEP | 60.53 | 27.69 | 4 |
| Kovk | KOV/CE | GAW/EMEP | 46.12 | 15.11 | 600 | Vorhegg | CE | EMEP | 46.68 | 12.97 | 1020 |
| K-puszta | CE | EMEP | 46.97 | 19.58 | 125 | Vredepeel | NE | EMEP | 51.54 | 5.85 | 28 |
| Krvavec | CE | EMEP | 46.30 | 14.54 | 1740 | Waldhof | WAL/NE | GAW/EMEP | 52.80 | 10.77 | 74 |
| La Coulonche | CE | EMEP | 48.63 | −0.45 | 309 | Westerland | WES/NE | GAW/EMEP | 54.93 | 8.32 | 12 |
| La Tardière | CE | EMEP | 46.65 | −0.75 | 143 | Weybourne | NE | EMEP | 52.95 | 1.12 | 16 |
| Lac La Biche | LAC | GAW | 54.95 | −112.45 | 540 | Wicken Fen | NE | EMEP | 52.30 | −0.29 | 5 |
| Ladybower Res. | NE | EMEP | 53.40 | −1.75 | 420 | Yarner Wood | NE | EMEP | 50.59 | −3.71 | 119 |
| Lahemaa | NE | EMEP | 59.50 | 25.90 | 32 | Yonagunijima | YON | GAW | 24.47 | 123.02 | 30 |
| Lauder | LAU | GAW | −45.03 | 169.67 | 370 | Zarodnje | CE | EMEP | 46.42 | 15.00 | 770 |
| Le Casset | CE | EMEP | 45.00 | 6.47 | 750 | Zarra | SE | EMEP | 39.09 | −1.10 | 885 |
| Leba | NE | EMEP | 54.75 | 17.53 | 2 | Zavodnje | ZAV | GAW | 46.43 | 15.00 | 770 |
| Lerwick | NE | EMEP | 60.13 | −1.18 | 85 | Zillertaler Alpen | CE | EMEP | 47.14 | 11.87 | 1970 |
| Lille Valby | NE | EMEP | 55.69 | 12.13 | 10 | Zingst | ZIN/NE | GAW/EMEP | 54.43 | 12.73 | 1 |
| Lough Navar | NE | EMEP | 54.44 | −7.87 | 126 | Zoebelboden | CE | EMEP | 47.83 | 14.44 | 899 |
| Lullington Heath | NE | EMEP | 50.79 | 0.17 | 120 | Zoseni | ZOS/NE | GAW/EMEP | 57.13 | 25.90 | 188 |
| Mace Head | NE | EMEP | 53.17 | −9.50 | 15 | Zugspitze | SFH | GAW | 47.42 | 10.98 | 2656 |
| Market Harborough | NE | EMEP | 52.55 | −0.77 | 145 | | | | | | |



**Table 4.** Modified normalized mean bias (MNMB) [%], correlation coefficient (*R*), and root mean square error (RMSE) [ppb] derived from the evaluation of the MACC_osuite with Global Atmospheric Watch (GAW) CO surface observations during the period September 2009 to December 2012.

| Station | ALT | BEO | CAP | CHI | CVO | EGB | ESP | ETL | FRA | IZO | JFJ | KOS | KOW | KRV | LAC | MCI | MNM |
|---|---|---|---|---|---|---|---|---|---|---|---|---|---|---|---|---|---|
| MNMB | −6.9 | −36.1 | 29.7 | −7.3 | −0.6 | 4.5 | −1.7 | −19.9 | −12.0 | −6.8 | −15.1 | −50.1 | −5.9 | −30.4 | −24.2 | −19.0 | 6.4 |
| *R* | 0.5 | 0.0 | 0.6 | 0.4 | 0.7 | 0.3 | 0.5 | 0.1 | 0.3 | 0.7 | 0.6 | 0.2 | 0.4 | 0.4 | 0.0 | 0.6 | 0.8 |
| RMSE | 23.4 | 90.3 | 20.4 | 31.1 | 14.2 | 60.1 | 25.7 | 53.9 | 35.9 | 15.3 | 25.8 | 131.1 | 70.1 | 49.1 | 58.5 | 32.0 | 22.0 |
| Station | NGW | PAY | PIC | PUY | RIG | RYO | SAB | SBL | SCH | SFH | USH | YON | | | | | |
| MNMB | −1.7 | −7.3 | −9.3 | −10.4 | 28.2 | −4.8 | −8.1 | −25.1 | −15.8 | −25.7 | −9.1 | −1.6 | | | | | |
| *R* | 0.4 | 0.3 | 0.7 | 0.6 | 0.0 | 0.4 | 0.4 | 0.5 | 0.5 | 0.4 | 0.6 | 0.7 | | | | | |
| RMSE | 61.6 | 99.2 | 18.4 | 30.6 | 143.5 | 44.5 | 31.6 | 36.8 | 39.8 | 45.0 | 12.3 | 62.3 | | | | | |

**Table 5.** Statistics derived from satellite observations (SCIAMACHY from September 2009 until March 2012, GOME-2 from April 2012 to December 2012) and the MACC_osuite simulations of daily tropospheric $NO_2$ VCD [$10^{15}$ molec cm$^{-2}$] averaged over different regions for September 2009 to December 2012.

| Region | United States | Europe | South Asia | East Asia | South Africa | North Africa |
|---|---|---|---|---|---|---|
| Model mean $NO_2$ VCD [$10^{15}$ molec cm$^2$] | 2.591 | 2.135 | 1.044 | 2.401 | 0.762 | 0.872 |
| Satellite mean $NO_2$ VCD [$10^{15}$ molec cm$^2$] | 3.066 | 3.596 | 1.225 | 6.145 | 1.072 | 0.887 |
| Modified normalized mean bias (MNMB) [%] | −16.628 | −49.276 | −14.409 | −69.852 | −38.21 | −4.601 |
| Root mean square error (RMSE) [$10^{15}$ molec cm$^2$] | 1.173 | 1.997 | 0.312 | 5.987 | 0.476 | 0.27 |
| Correlation coefficient ($R$) [dimensionless] | 0.567 | 0.781 | 0.744 | 0.84 | 0.606 | 0.455 |



**Table 6.** Modified normalized mean bias (MNMB) [%], correlation coefficient ($R$), and root mean square error (RMSE) [ppb] derived from the evaluation of the MACC_osuite with Global Atmosphere Watch (GAW) $O_3$ surface observations during the period September 2009 to December 2012.

| Station | ARH | ASS | BAH | BAR | BEO | CAI | CAG | CAP | CVO | CON | DOB | EVP | ISK | IZO | JFJ | KOW | KOS |
|---|---|---|---|---|---|---|---|---|---|---|---|---|---|---|---|---|---|
| MNMB | −39.8 | −6.3 | −8.6 | −35.1 | −21.4 | 70.1 | −12.7 | 13.7 | 15.2 | −81.6 | 6.3 | 18.4 | 67.2 | 10.4 | 1.9 | 5.8 | −5.9 |
| $R$ | 0.6 | 0.7 | 0.5 | 0.3 | 0.4 | −0.1 | 0.4 | 0.6 | 0.6 | 0.3 | 0.3 | 0.7 | 0.1 | 0.5 | 0.7 | 0.6 | 0.6 |
| RMSE | 10.6 | 6.5 | 8.0 | 13.8 | 20.4 | 29.2 | 8.9 | 7.6 | 8.0 | 17.2 | 14.3 | 12.0 | 34.5 | 10.8 | 7.4 | 12.0 | 16.3 |
| Station | KOV | KRV | LAU | MAU | MNM | MCI | NGW | NEU | PAY | PIC | PUY | RAG | RIG | RUC | RYO | SCH | SBL |
| MNMB | 21.2 | 9.5 | −5.5 | 13.7 | 38.6 | 2.3 | −11.4 | −45.2 | −28.8 | 5.5 | 12.8 | 38.6 | −80.3 | −0.1 | 10.5 | 8.5 | 8.1 |
| $R$ | 0.6 | 0.6 | 0.5 | 0.6 | 0.8 | 0.7 | 0.5 | 0.5 | 0.7 | 0.6 | 0.6 | 0.6 | 0.3 | 0.3 | 0.1 | 0.7 | 0.6 |
| RMSE | 19.5 | 11.1 | 9.0 | 11.5 | 13.0 | 8.2 | 14.3 | 11.4 | 15.6 | 7.7 | 10.6 | 10.6 | 28.4 | 15.0 | 14.4 | 12.2 | 9.3 |
| Station | SFH | SPO | SUM | SYO | TRI | TSU | TUD | TUT | USH | VIN | WAL | WES | YON | ZAV | ZIN | ZOS | |
| MNMB | 10.1 | −70.6 | −24.4 | −31.2 | 3.2 | 55.1 | 45.3 | 40.2 | −7.0 | 4.6 | −18.0 | −12.3 | 22.0 | 19.7 | −17.5 | 22.3 | |
| $R$ | 0.6 | 0.4 | 0.5 | 0.7 | 0.3 | 0.0 | 0.5 | 0.8 | 0.5 | 0.4 | 0.6 | 0.6 | 0.7 | 0.6 | 0.4 | 0.2 | |
| RMSE | 9.3 | 16.3 | 11.7 | 8.9 | 13.3 | 27.6 | 18.2 | 8.0 | 7.6 | 11.2 | 13.6 | 11.6 | 13.6 | 18.6 | 13.9 | 17.0 | |

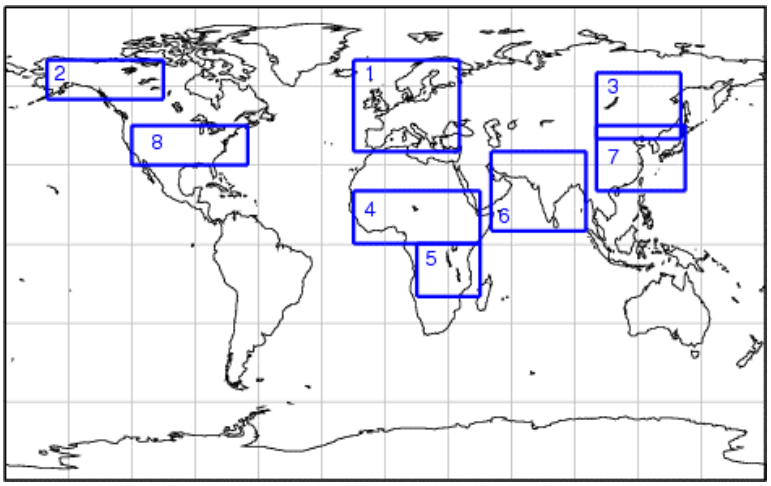


**Figure 1.** Regions used for regional data-stratification in the troposphere for the comparison with satellite data. The following regions are defined: **1** Europe (15° W–35° E, 35–70° N), **2** Fires-Alaska (150–105° W, 55–70° N), **3** Fires-Siberia (100–140° E, 40–65° N), **4** North Africa (15° W–45° E, 0–20° N), **5** South Africa (15–45° E, 20–0° S), **6** South Asia (50–95° E, 5–35° N), **7** East Asia (100–142° E, 20–45° N), **8** United States (120–65° W, 30–45° N).





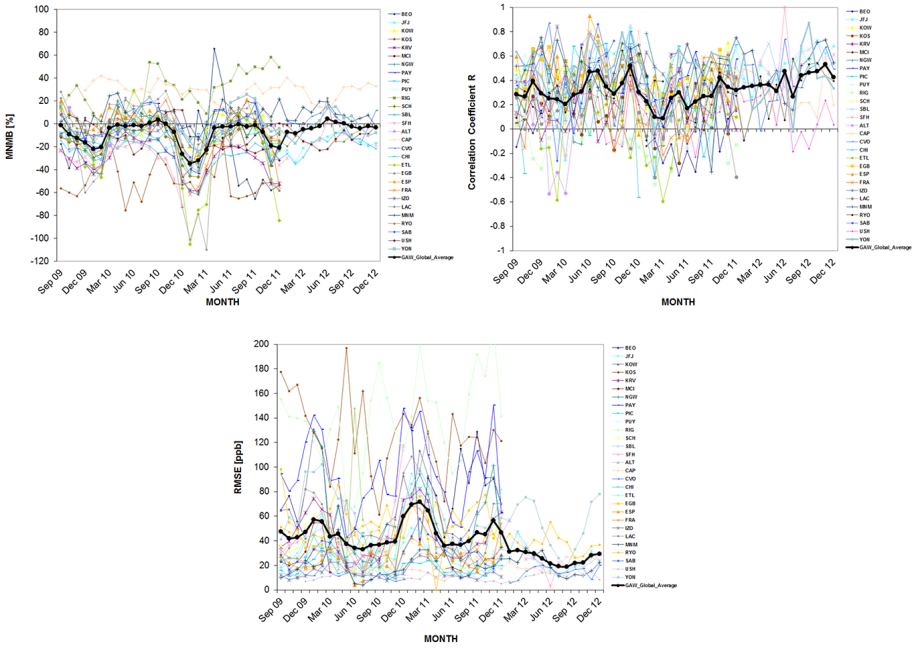


**Figure 2. (a)** Modified normalized mean bias (MNMB) in % (top left) and correlation coefficient ($R$), (top right) derived from the evaluation of the MACC_osuite with GAW CO surface observations over the period September 2009 to December 2012 (black line: global average of 29 GAW stations. Multi-coloured lines: individual station results, see legend to the right). **(b)** Root mean square error (RMSE) in ppb derived from the evaluation of the MACC_osuite with GAW CO surface observations over the period September 2009 to December 2012 (black line: global average of 29 GAW stations multi-coloured lines: individual station results, see legend to the right).

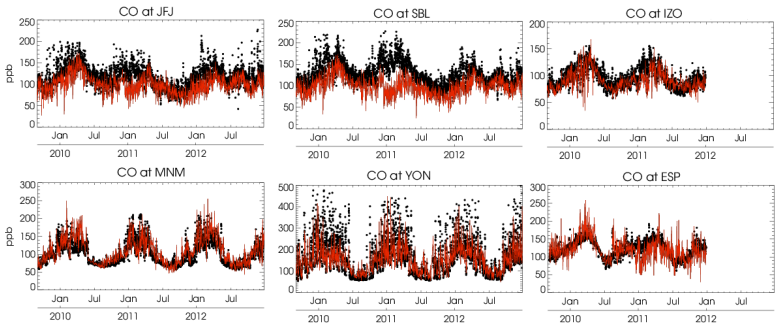


**Figure 3.** Time series plots of the MACC_osuite 6 hourly CO mixing ratios (red) and GAW surface observations (black) for Jungfraujoch – JFJ (Switzerland), Sonnblick – SBL (Austria), Izana Observatory – IZO (Tenerife), Minamitorishima – MNM (Japan), Yonagunijima – YON (Japan), Estevan Point – EVP (Canada) during the period September 2009 to December 2012. Unit: ppb.





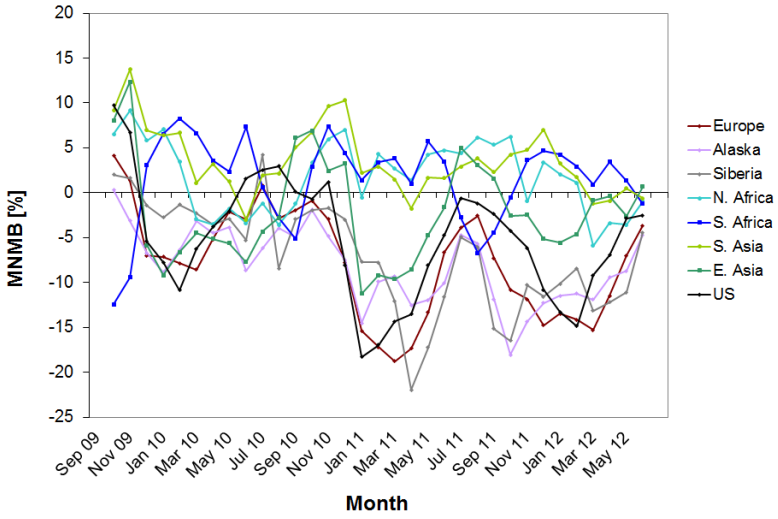


**Figure 4.** Monthly average of modified normalized mean biases (MNMBs) derived from the comparison of the MACC_osuite with MOPITT CO total columns for 8 different regions during the period September 2009 to June 2012 (see legend on the right).

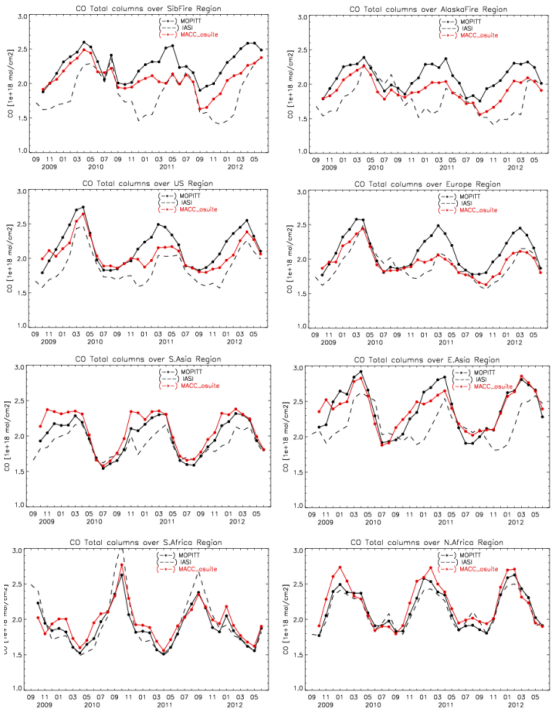


**Figure 5.** Time series plots of MOPITT CO total columns (black line) compared to IASI CO total columns (black dashed line) and the MACC_osuite CO total columns (red line) for 8 different regions (defined in Fig. 1) during the period September 2009 to June 2012. Top: Fires-Siberia (left), Fires-Alaska (right), second row: United States (left), Europe (right), third row: South Asia (left), East Asia (right) bottom: South Africa (left), North Africa (right).



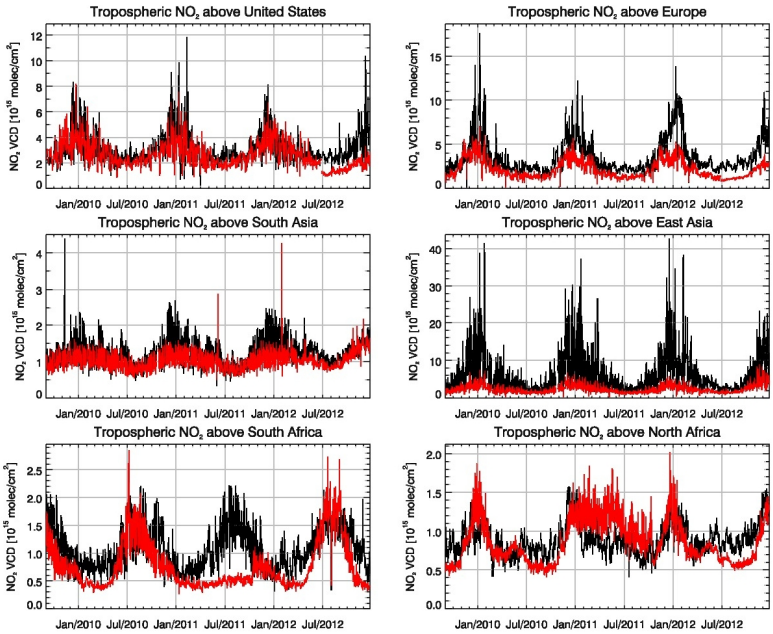


**Figure 6.** Time series of daily tropospheric $NO_2$ VCD [$10^{15}$ molec cm$^{-2}$] averaged over different regions. Top: United States (left), Europe (right), second row: South Asia (left), East Asia (right), bottom: South Africa (left), North Africa (right). Black lines show satellite observations (SCIAMACHY up to March 2012, GOME-2 from April 2012 to December 2012), red lines correspond to the MACC_osuite simulations.

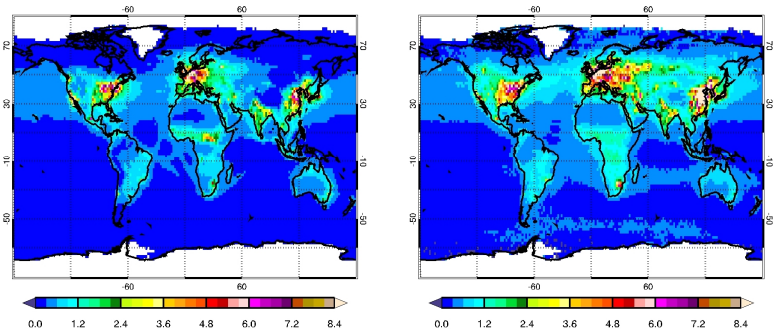


**Figure 7.** Long-term average of daily tropospheric $NO_2$ VCD [$10^{15}$ molec cm$^{-2}$] from September 2009 to March 2012 for (left) MACC_osuite simulations and (right) SCIAMACHY satellite observations. Blue colours represent low values; red/brown colours represent high values.





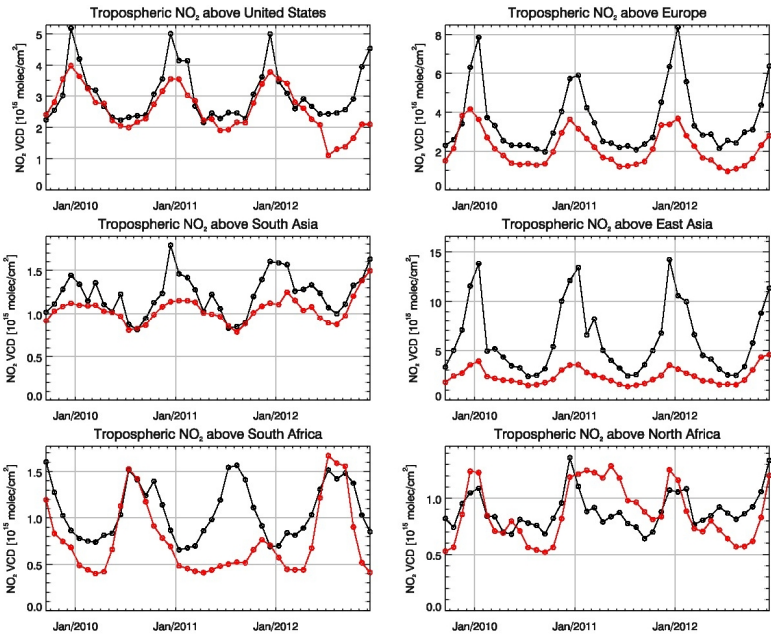


**Figure 8.** As in Fig. 6 but for monthly means of daily tropospheric $NO_2$ VCD [$10^{15}$ molec cm$^{-2}$] averaged over different regions. Top: United States (left), Europe (right), second row: South Asia (left), East Asia (right), bottom: South Africa (left), North Africa (right).

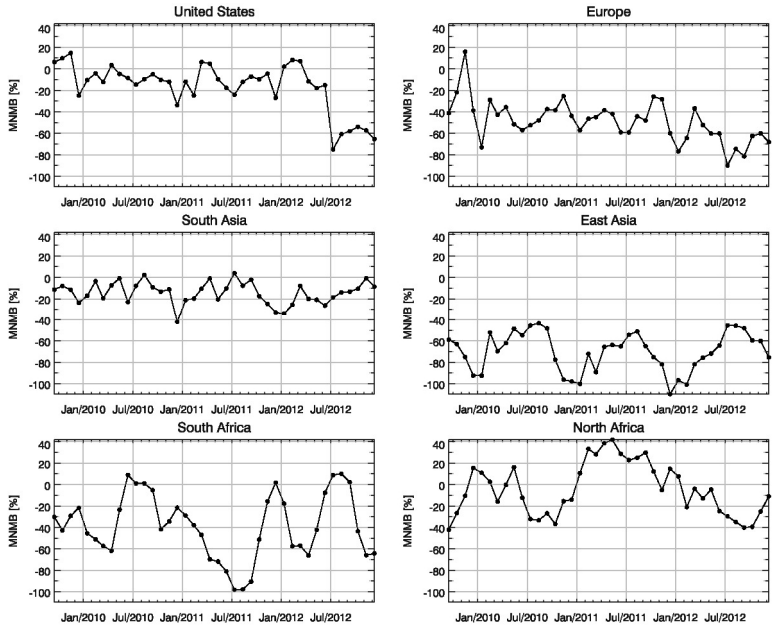


**Figure 9.** Modified normalized mean bias [%] of daily tropospheric $NO_2$ VCD averaged over different regions (see text for latitudinal and longitudinal boundaries) derived from the MACC_osuite simulations and satellite observations (SCIAMACHY up to March 2012, GOME-2 from April 2012 to December 2012). Top: United States (left), Europe (right), second row: South Asia (left), East Asia (right), bottom: South Africa (left), North Africa (right).Values have been calculated separately for each month.



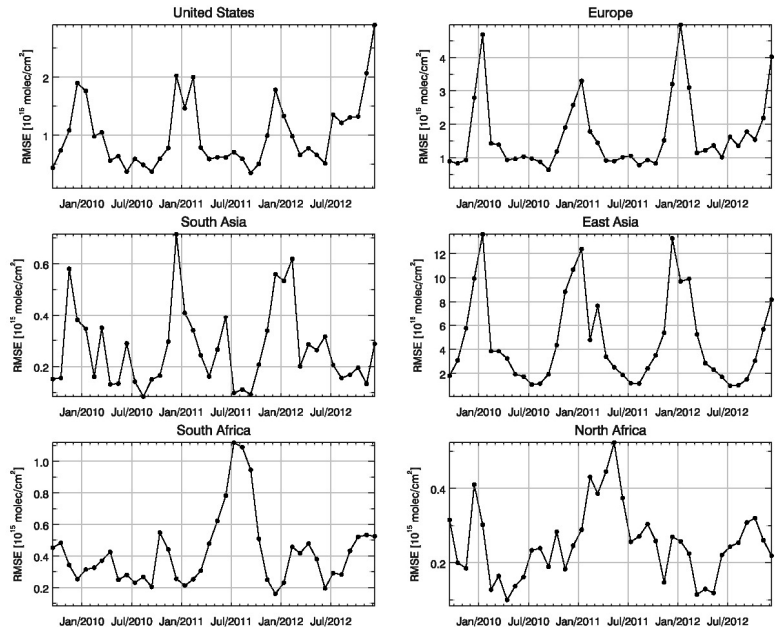


**Figure 10.** As in Fig. 9 but for the root mean square error [$10^{15}$ molec cm$^{-2}$].

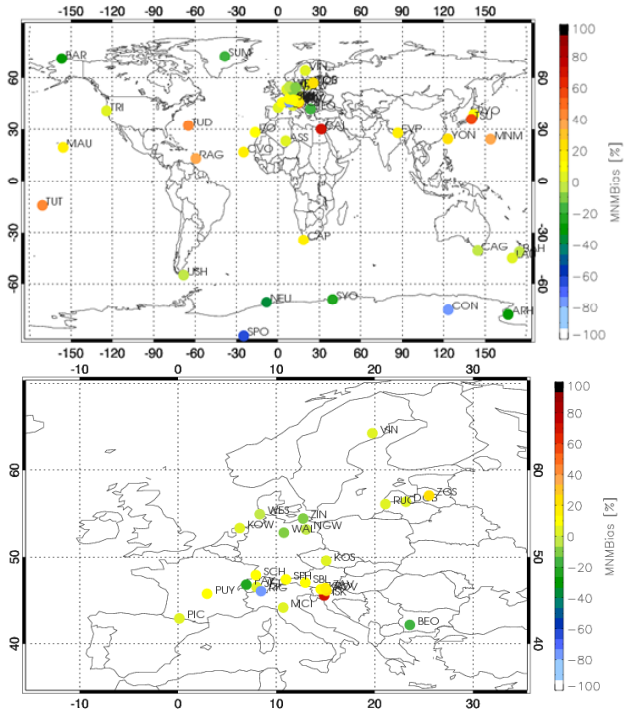


**Figure 11.** Modified normalized mean biases (MNMBs) [%] derived from the evaluation of the MACC_osuite with GAW $O_3$ surface observations during the period September 2009 to December 2012 globally (top), and for Europe (below). Blue colours represent large negative values; red/brown colours represent large positive values.



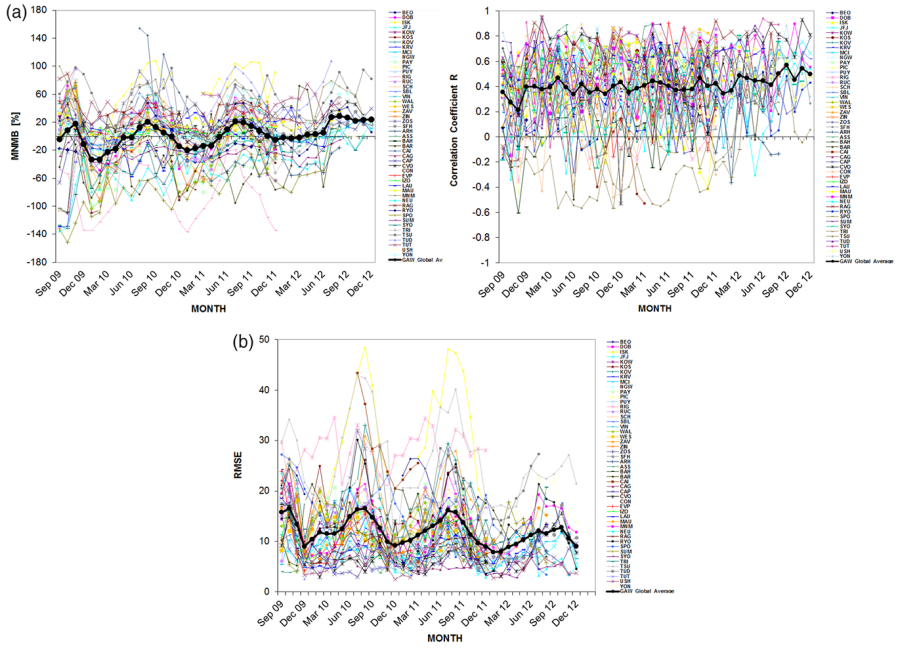


**Figure 12. (a)** Modified normalized mean bias (MNMB) in % (top left) and correlation coefficient ($R$), (top right) derived from the evaluation of the MACC_osuite with GAW $O_3$ surface observations during the period September 2009 to December 2012 (black line: global average of 50 GAW stations. Multi-coloured lines: individual station results, see legend to the right). **(b)** Root mean square error (RMSE) in ppb derived from the evaluation of the MACC_osuite with GAW $O_3$ surface observations during the period September 2009 to December 2012 (black line: global average of 50 GAW stations. Multi-coloured lines: individual station results, see legend to the right).

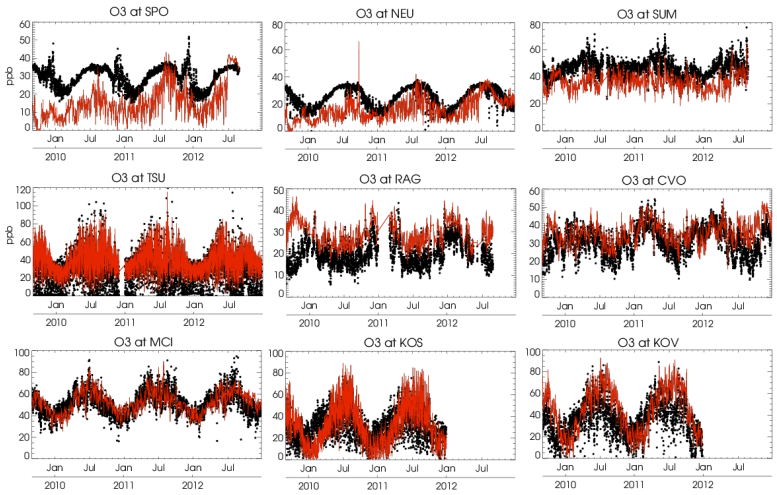


**Figure 13.** Time series plots of the MACC_osuite 6 hourly $O_3$ mixing ratios (red) and GAW surface observations (black) for South Pole – SPO (Antarctica), Neumayer – NEU (Antarctica), Summit – SUM (Denmark), Tsukuba – TSU (Japan), Ragged Point – RAG, (Barbados), Cape Verde Observatory – CVO (Cape Verde), Monte Cimone – MCI (Italy), Kosetice – KOS (Czech Republic), Kovk – KOV (Slovenia) during the period September 2009 to December 2012. Unit: ppb.



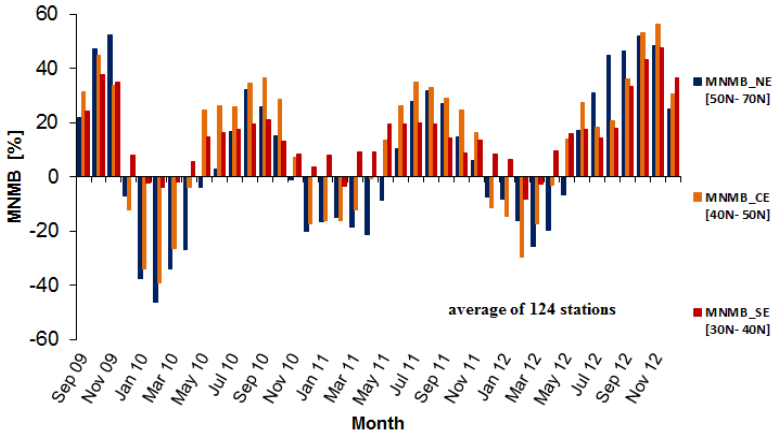


**Figure 14.** Modified normalized mean biases (MNMBs) derived from the evaluation of the MACC_osuite with EMEP $O_3$ surface observations in three different parts in Europe (blue: Northern Europe, orange: Central Europe, red: Southern Europe) during the period September 2009 to December 2012.

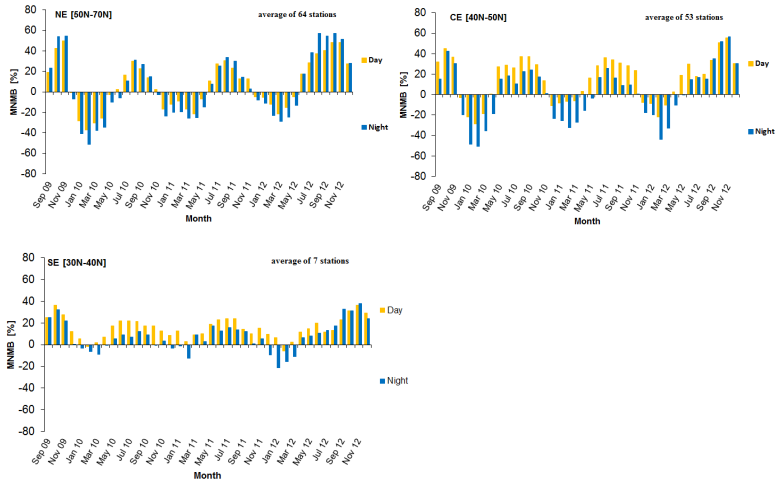


**Figure 15.** Modified normalized mean biases (MNMBs) derived from the evaluation of the MACC_osuite with EMEP $O_3$ surface observations during day-time (yellow color), and night-time (blue color) over northern Europe (top left), central Europe (top right) and southern Europe (bottom) during the period September 2009 to December 2012.